Table III. Chemical Shifts of Leu F4/89 in metMbCN

spins	δ_{obs}[a]	δ^*_{pre}[b]	δ^+_{pre}[c]	δ_{dia}[d]	δ_{dip}[e]	slope ($\times 10^{-3}$)[f]
$C_\alpha H$	8.68	8.46	8.46	3.74	4.94	2.76
$C_{\beta 1} H$	4.51	3.82	3.82	1.48	3.03	1.62
$C_{\beta 2} H$	3.85	3.12	3.12	1.18	2.67	1.14
$C_\gamma H$	6.02	4.86	7.76	0.63	5.39	3.14
$C_{\delta 1} H_3$	4.07	1.86	3.77	0.31	3.76	2.67
$C_{\delta 2} H_3$	3.34	10.36	1.96	0.44	2.90	1.81

[a] Experimentally observed chemical shifts in ppm from DSS at 25 °C in ^2H_2O at pH*8.6. [b] Predicted chemical shifts at 25 °C relative to DSS, $\delta^*_{pre} = \delta_{dia} + \delta_{dip}$(calc), where δ_{dip}(calc) is computed by using the crystal structure orientation of Leu F4; taken from ref 6. [c] Predicted chemical shifts at 25 °C, relative to DSS, $\delta^+_{pre} = \delta_{dia} + \delta_{dip}$(calc), where δ_{dip}(calc) is calculated from the new orientation of the Leu F4 side chain which best reproduces the data (Figure 6). [d] Diamagnetic shifts obtained from MbCO at 36 °C and pH* 5.6 (ref 33). [e] The experimentally observed dipolar shift, $\delta_{dip} = \delta_{obs} - \delta_{dia}$. [f] Slopes were measured from the variable-temperature behavior of the experimentally observed chemical shifts, $\Delta\delta/\Delta(1/T)$ in ppm °C; see ref 6.

Leu F4 lies on the proximal side of the heme adjacent to the "xenon hole", a hydrophobic vacancy over pyrrole I, and hence has available to it significant conformational flexibility, particularly about the C_β–C_γ bond, without disrupting neighboring residues.[20,33] To ascertain whether the failure to predict correctly the Leu F4 dipolar shift is due to a distinct alternate orientation, we calculated both the dipolar shifts and expected NOEs between the Leu terminal methyls and the heme 1-CH_3 (i.e., [r(heme 1-CH_3–Leu F4 $C_{\delta 2}H_3$)/r(heme 1-CH_3–Leu F4 $C_{\delta 1}H_3$)][6]) as a function of the C_β–C_γ rotational angle; the results for these calculations are presented in Figure 6. It is clear from this figure that rotation about the C_β–C_γ by $-120 \pm 20°$ not only reproduces reasonably both the pattern and magnitudes of the Leu F4 shifts (δ^+_{pre} at $-120°$ rotational angle; see Table III) but also places both methyls within comparable NOE distance of the heme 1-CH_3, as observed. Moreover, the slopes of the experimental dipolar shifts, derived from variable-temperature COSY maps, are proportional to the dipolar shifts, δ_{dip} (Table III), as found earlier for all other dipolar shifted residues[6] and hence argue not only that the orientation of Leu F4 in metMbCN in solution is different from that of MbCO in the crystal but also that this orientation with C_β–C_γ rotated by $\sim 120°$ is likely the dominant one. It is of interest that the reoriented Leu F4 presently characterized in solution of sperm whale metMbCN is close to that found in the crystal structure of horse metMb:[48] the horse and sperm whale Mb crystal structures are otherwise isostructural on the proximal side of the heme pocket. Hence this residue provides a dramatic example of the problem that can arise when solution NOESY data are interpreted too closely on the basis of crystal coordinates and reaffirms the absolute necessity for the independent amino acid spin connectivity assignments provided by the present study.

Acknowledgment. The authors are indebted to S. D. Emerson who wrote the computer programs for dipolar shift calculations. This research is fully supported by a grant from the National Institutes of Health, HL-16087.

(48) Evans, S. V.; Brayer, G. D. *J. Biol. Chem.* **1988**, *263*, 4263-4268.

Spectroscopic and Chemical Studies of the Laccase Trinuclear Copper Active Site: Geometric and Electronic Structure

James L. Cole, Patrick A. Clark, and Edward I. Solomon*

Contribution from the Department of Chemistry, Stanford University, Stanford, California 94305.
Received June 28, 1990

Abstract: Laccase contains four Cu atoms: a type 1, a type 2, and a coupled binuclear type 3 center. The type 2 and type 3 centers comprise a trinuclear Cu cluster which is thought to represent the active site for the binding and multielectron reduction of dioxygen. A combination of electronic spectroscopy, magnetic susceptibility, and exogenous ligand perturbation has been used to probe the geometric and electronic structure of the trinuclear site. A type 1 Hg^{2+}-substituted laccase derivative was employed in order to remove the overlapping spectral contributions from the type 1 Cu^{2+}. The ligand-field and charge-transfer transitions of the type 2 and type 3 coppers were assigned by use of absorption, circular dichroism, and low-temperature magnetic circular dichroism spectroscopies. The ligand-field transition energies indicate that all three coppers have tetragonal geometries and that the two type 3 coppers are inequivalent. Magnetic susceptibility measurements have defined the lower limit for the magnitude of the exchange interaction between the type 3 coppers and have probed type 2–type 3 interactions. Binding of the exogenous ligand azide to the trinuclear site produces characteristic azide $\rightarrow Cu^{2+}$ charge-transfer features and also perturbs the type 2 and type 3 ligand-field transitions. Analysis of these spectral features demonstrates that azide binds as a bridging ligand between the type 2 site and one of the type 3 coppers. In addition, a second azide coordinates to the type 3 site with a lower binding constant, and this second azide also strongly interacts with the type 2 site. The type 2–type 3 bridged binding of azide suggests that a similar coordination mode is active in the irreversible binding and four-electron reduction of dioxygen. The second azide binding provides a further demonstration of the differences between the laccase type 3 site and the coupled binuclear sites in hemocyanin and tyrosinase. A model for the magnetic interactions among the three coppers in the resting and ligand bound forms of the trinuclear site is presented.

Introduction

The multicopper oxidases[1,2] laccase, ascorbate oxidase, and ceruloplasmin catalyze the four-electron reduction of dioxygen to water. The Cu atoms present in these enzymes have been classified[1] according to their EPR features: type 1 or blue ($A_\parallel \leq 95 \times 10^{-4}$ cm^{-1}), type 2 or normal ($A_\parallel > 140 \times 10^{-4}$ cm^{-1}), and type 3 or coupled binuclear (EPR undetectable). The type 3 coppers are strongly antiferromagnetically coupled so that the type 3 site is diamagnetic, even at room temperature.[3] The super-exchange interaction is mediated by an endogenous bridging ligand OR^-.[2] The various copper sites also give rise to characteristic

(1) (a) Malkin, R.; Malmström, B. G. *Adv. Enzymol.* **1970**, *33*, 177. (b) Malmström, B. G.; Andréasson, L.-E.; Reinhammar, B. In *The Enzymes*; Boyer, P. D., Ed.; Academic: New York, 1975; Vol. XII. (c) Fee, J. A. *Struct. Bonding (Berlin)* **1975**, *23*, 1-60.

(2) Solomon, E. I.; Penfield, K. W.; Wilcox, D. E. *Struct. Bonding (Berlin)* **1983**, *53*, 1.

(3) Dooley, D. M.; Scott, R. A.; Ellinghaus, J.; Solomon, E. I.; Gray, H. B. *Proc. Natl. Acad. Sci. U.S.A.* **1978**, *75*, 3019-3022.

0002-7863/90/1512-9534$02.50/0

electronic absorption features. The type 1 site exhibits an intense $S \rightarrow Cu^{2+}$ charge-transfer band near 600 nm ($\Delta\epsilon \sim 5000$ M^{-1} cm^{-1}) and several weaker features from the UV to the near-IR region.[4] The oxidized type 3 site displays a broad near UV absorption band maximizing at 330 nm, $\Delta\epsilon = 2800$ M^{-1} cm^{-1},[5] and a d $\rightarrow$ d band at 740–745 nm.[6] No absorption features have been assigned to the type 2 site.

Much of the spectroscopic and mechanistic research on these enzymes has focused on laccase because it is the simplest multicopper oxidase, containing one type 1, one type 2, and one binuclear type 3 site (four copper atoms). We have determined through low-temperature magnetic circular dichroism (MCD) studies that the exogenous anionic inhibitor N_3^- binds to laccase as a bridging ligand between the type 2 and type 3 sites, thereby defining a novel trinuclear copper cluster. It was suggested that this trinuclear site represents the true active site for the binding and multielectron reduction of dioxygen.[7] Ascorbate oxidase contains two subunits and two of each type of copper site.[8] This enzyme has been crystallized, and a recent 2.5-Å X-ray structure confirms this trinuclear model by showing that each subunit contains three copper atoms within 3.9 Å of each other and a type 1 Cu^{2+} site ~12 Å away from the trinuclear cluster.[9]

Two useful derivatives of laccase have been prepared by selective metal removal and substitution procedures. The type 2 Cu^{2+} may be selectively chelated, generating a derivative containing only the type 1 and type 3 sites; this form is referred to as type 2 depleted (T2D).[10] In addition, the type 1 Cu^{2+} may be selectively replaced by Hg^{2+}, leaving the type 2 and type 3 sites intact;[11] this form is referred to as type 1 Hg^{2+}-substituted (T1Hg). It has been demonstrated by X-ray absorption spectroscopy that T2D laccase contains a reduced type 3 site,[6a,12] and this form is referred to as deoxy-T2D. The type 3 site can be oxidized by H_2O_2, but not by dioxygen, generating met-T2D laccase, and one-electron reduction of met-T2D generates half-met-T2D.[13] Ligand-binding studies of the met and half-met forms indicate that, unlike hemocyanin and tyrosinase, exogenous ligands do not bridge the type 3 site in T2D laccase.[13] In contrast to T2D laccase, T1Hg laccase is fully oxidized after preparation.[14] It has been demonstrated that the presence of the type 2 site is necessary for reactivity of the type 3 site with dioxygen, and that the type 2–type 3 trinuclear center in T1Hg laccase represents the minimal structural unit capable of reducing dioxygen.[14] It has also been shown that the unusually high affinity of fluoride for the type 2 site in native laccase is preserved in T1Hg laccase.[15] These results clearly show that the T1Hg derivative contains a valid trinuclear site.

In the present study, absorption, CD, and MCD spectroscopies and exogenous ligand perturbations are used to probe the electronic and geometric structure of the type 2–type 3 trinuclear active site. The type 1 Cu^{2+} site in native laccase produces intense spectral features, which obscure the low-energy region that contains the Cu^{2+} d $\rightarrow$ d bands associated with the type 2–type 3 trinuclear site. Such information is crucial to our understanding of the trinuclear site, because the d $\rightarrow$ d bands probe the electronic and geometric structure of the type 2 and type 3 sites, and they also reveal exogenous ligand-induced distortions of the trinuclear site. We have circumvented this problem by using T1Hg laccase, because the Hg^{2+} ion in the type 1 binding site does not exhibit spectral features in the region of interest (from 300 to 1100 nm). An additional benefit of the T1Hg derivative is that the type 3 site is completely oxidized, whereas in native laccase 22% of the type 3 sites are reduced.[12] These reduced type 3 sites are associated high-affinity ($K \geq 10^4$ M^{-1}) N_3^- binding, which complicates observation of the low-affinity ($K \sim 200$ M^{-1}) N_3^- that binds as a bridging ligand between the oxidized type 2 and type 3 sites.[7]

MCD is extremely useful in discriminating between the type 2 and type 3 electronic transitions in the trinuclear site. The magnetic ground state associated with an observed electronic transition may be determined by examining the temperature dependence of the corresponding MCD feature: magnetically degenerate ground states give rise to MCD bands whose intensities are proportional to $1/T$ for $kT \gg g\beta H$ (C term), while MCD features associated with magnetically nondegenerate ground states are temperature independent (A and B terms). The type 2 site is magnetically degenerate ($S = {}^1/_2$), whereas the type 3 consists of a pair of antiferromagnetically coupled Cu^{2+} ions with a magnetically nondegenerate ground state with $S_{total} = 0$ (the $S_{total} = 1$ state is not significantly populated for $T < 300$ K because the type 3 site is very strongly coupled).[3] Near 4 K, the MCD features associated with the diamagnetic type 3 site will be 100–1000 times weaker than those from the paramagnetic type 2 center; therefore, the MCD spectrum of T1Hg laccase will be dominated by contributions from the type 2 Cu^{2+}. It is also observed that upon binding azide the endogenous bridge is displaced in <10% of the type 2 sites. This disrupts the antiferromagnetic coupling, giving rise to additional MCD features from the uncoupled type 3 sites. These features can easily be recognized by a characteristic dependence on $[N_3^-]$ (vide infra).

In this study, we have assigned the ligand-field and charge-transfer transitions of the type 2 and type 3 coppers using absorption, circular dichroism, and low-temperature MCD spectroscopies, and these data provide new insights into the electronic structure of the trinuclear site. Magnetic susceptibility measurements have probed the exchange coupling within the trinuclear site. Detailed spectral studies are presented that demonstrate that the exogenous ligand N_3-binds to the trinuclear site by bridging the type 2 and one of the type 3 coppers, and further, a second azide binds to the type 3 site with a lower binding constant and strongly interacts with the type 2 copper. A model for the magnetic interactions among the three coppers in the resting and ligand bound forms of the trinuclear site is presented.

Experimental Section

Rhus vernificera laccase was isolated[16] from the acetone powder (Saito and Co., Osaka, Japan) to a purity ratio A_{280}/A_{614} of 14.5–15.5, as modified in ref 13. Laccase activity was assayed spectrophotometrically by using *N,N*-dimethyl-*p*-phenylenediamine as the substrate.[16] The T1Hg derivative of laccase was prepared according to published procedures[11] as modified in ref 14. The concentration of T1Hg was assayed by using the absorption band at 280 nm, and the extinction coefficient was determined for each preparation on the basis of the A_{280}/A_{614} ratio of the native laccase ($\epsilon_{614} = 5700$ M^{-1} cm^{-1}). This method agrees within 10% with the Bradford dye binding assay,[17] using native laccase as a standard. The type 2 depleted (T2D) laccase was prepared according to the procedure of Graziani et al.[10] as modified in ref 13. Copper concentration was determined by atomic absorption spectroscopy. Samples for MCD spectroscopy were concentrated to ~0.25 mM with Immersible-CX ultrafilters (Millipore Corp., Bedford, MA) and were subsequently dialyzed against 50% (v/v) glycerol–0.2 M potassium phosphate, pH 6.0, buffer, which provides a good quality low-temperature

(4) Gewirth, A. A.; Solomon, E. I. *J. Am. Chem. Soc.* **1988**, *110*, 3811–3819, and references therein.
(5) Reinhammar, B. R. M. *Biochim. Biophys. Acta* **1972**, *275*, 245–259.
(6) (a) LuBien, C. D.; Winkler, M. E.; Thamann, T. J.; Scott, R. A.; Co, M. S.; Hodgson, K. O.; Solomon, E. I. *J. Am. Chem. Soc.* **1981**, *103*, 7014–7016. (b) Tamilarasan, R.; McMillin, D. R. *Biochem. J.* **1989**, *263*, 425–429.
(7) (a) Allendorf, M. D.; Spira, D. J.; Solomon, E. I. *Proc. Natl. Acad. Sci. U.S.A.* **1985**, *82*, 3063–3067. (b) Spira-Solomon, D. J.; Allendorf, M. D.; Solomon, E. I. *J. Am. Chem. Soc.* **1986**, *108*, 5318–5328.
(8) Morpurgo, L.; Savini, I.; Gatti, G.; Bolognesi, M.; Avigliano, L. *Biochem. Biophys. Res. Commun.* **1988**, *152*, 623–628.
(9) (a) Messerschmidt, A.; Rossi, A.; Ladenstein, R.; Huber, R.; Bolognesi, M.; Gatti, G.; Marchesini, A.; Petruzzelli, R.; Finazzi-Agrò, A. *J. Mol. Biol.* **1989**, *206*, 513–529. (b) Messerschmidt, A.; Huber, R. *Eur. J. Biochem.* **1990**, *187*, 341–352.
(10) Graziani, M. T.; Morpurgo, L.; Rotilio, G.; Mondovì, B. *FEBS Lett.* **1976**, *70*, 87–90.
(11) Morie-Bebel, M. M.; Morris, M. C.; Menzie, J. L.; McMillin, D. R. *J. Am. Chem. Soc.* **1984**, *106*, 3677–3678.
(12) Kau, L.-S.; Spira-Solomon, D. J.; Penner-Hahn, J. E.; Hodgson, K. O.; Solomon, E. I. *J. Am. Chem. Soc.* **1987**, *109*, 6433–6442.
(13) Spira-Solomon, D. J.; Solomon, E. I. *J. Am. Chem. Soc.* **1987**, *109*, 6421–6432.
(14) Cole, J. L.; Tan, G. O.; Yang, E. K., Hodgson, K. O.; Solomon, E. I. *J. Am. Chem. Soc.* **1990**, *112*, 2243–2249.
(15) Morie-Bebel, M. M.; McMillin, D. R.; Antholine, W. E. *Biochem. J.* **1986**, *235*, 415–420.
(16) Reinhammar, B. *Biochim. Biophys. Acta* **1970**, *205*, 35–47.
(17) Bradford, M. *Anal. Biochem.* **1976**, *72*, 248.

glass. The dialysis step further concentrated the samples to ~0.6 mM. All TlHg derivative was used within 1 week of preparation. A paramagnetic Cu^{2+} impurity was detected in the MCD and 77 K EPR spectra of samples that were aged for several weeks at 4 °C and the azide binding behavior was also perturbed. For anaerobic experiments, TlHg laccase was dialyzed against N_2-purged 100 mM potassium phosphate (pH 6.0) and was transferred to a N_2-purged cuvette for optical absorption and CD measurements. Samples for magnetic susceptibility were prepared in 100 mM potassium phosphate in D_2O, pH* 5.57. For ligand titration experiments, 5–10 μL of concentrated aqueous anion solutions were added to 150–200-μL aliquots of TlHg laccase, and samples were allowed to equilibrate at least 24 h prior to spectroscopic measurements. Azide binding constants were determined by the method of Byers et al.[18] All chemicals were reagent grade and were used without further purification. Water was purified to a resistivity of 15–18 MΩ cm with a Barnstead Nanopure deionizing system.

UV–visible absorption spectra were recorded at either 298 or 277 K on either a Cary 17 or a Hewlett-Packard HP8452A diode array spectrophotometer in 2-mm quartz cuvettes. Low-temperature absorption and MCD data were obtained by using a sample cell consisting of two quartz disks with a 1.5-mm rubber spacer. Samples were mounted on a laboratory-built optical Dewar for 77 K absorption measurements. Low-temperature MCD spectroscopy was performed with a Jasco J 500-C spectropolarimeter operating with S-1 and S-20 photomultiplier tubes for the 1100–800- and 800–300-nm regions, respectively, and an Oxford Spectromag 4 superconducting magnet/cryostat as previously described.[7] Samples at 298 K were cooled at a rate of ~1°/s to form an optical quality glass by using liquid helium from the sample cryostat. Strain-induced depolarization of the light by the sample glass was measured by comparing the CD spectra of a solution of nickel tartrate placed before and after the sample: depolarization of <10% was routinely obtained. Sample temperatures were measured with a calibrated carbon glass resistor (Cryogenic Calibrations, Pitchcott, Aylesbury, Buckinghamshire, U.K.). Spectra were generally obtained at 4 K and 5 T. MCD intensity is reported in units of $(M\ cm\ T)^{-1}$. EPR spectra were obtained with a Bruker ER 220-D-SRC spectrometer. Sample temperatures of 77–100 K were maintained with a liquid N_2 finger Dewar or a N_2 gas flow system, and temperatures from 4 to 70 K were obtained by using an Air Products Model LTR Helitran liquid helium transfer refrigerator and a Lake Shore Cryotronics temperature controller, Model DTC-500. The electronic and EPR spectra were smoothed for presentation by use of a Fourier filtering algorithm.[19]

Magnetic susceptibility measurements were taken on S.H.E. Model 905 SQUID magnetometers at the Francis Bitter National Magnet Laboratory at MIT and at the University of Southern California. An open Suprasil quartz bucket, which had been etched in 10% HF to remove surface paramagnetic impurities, was used for all magnetic measurements. Sample volumes were 100 μL, and both protein and background samples were dissolved in D_2O. The samples were suspended in the antechamber of the magnetometer by a cotton thread, and the antechamber was briefly flushed with He gas. The samples were then rapidly loaded into the cold magnetometer to prevent evaporative loss. Background measurements were made on the bucket containig deuterated buffer and these data were subtracted from the protein data to correct for the diamagnetism of the bucket and buffer and the paramagnetic contribution of dissolved dioxygen. The susceptibility versus $1/T$ data were fit in the 8–100 K region by a linear least-squares procedure. The data was adjusted to pass through the origin, thus correcting for the protein diamagnetism and the temperature-independent paramagnetism of the copper.

Results and Analysis

Electronic Spectroscopy of the Trinuclear Site: Type 2 Features. Figure 1A shows the low-temperature MCD spectrum of TlHg laccase in the region from 300 to 1100 nm. The amplitude of the MCD spectrum exhibits a $1/T$ temperature dependence from 4 to 150 K, and no additional features were detected at the higher temperatures (data not shown). Therefore, these features arise from a paramagnetic ground state (C term) and they are assigned to the type 2 site. Broad bands are observed at 860 (positive), 720 (negative), and 550 nm (negative) and several sharper bands are observed at 320, 345, 370, and 426 nm. In monomeric Cu^{2+} systems with N, O ligation, ligand → metal charge-transfer (CT) features generally occur at >20 000 cm^{-1} (<500 nm) and the d → d transitions occur at <20 000 cm^{-1}.[20] The features at 860, 720, and 550 nm in the MCD spectrum of TlHg laccase are thus assigned as d → d transitions. The amplitude of the 550-nm band (asterisk in Figure 1A) is variable: it increases upon ageing of the protein at 4 °C, and an additional $S = {}^1/_2$ Cu^{2+} signal is detectable in the EPR spectra of samples in which this MCD feature is prominent (data not shown). Thus, it is associated with a paramagnetic impurity in the preparation. This contaminant represents <10% of the total copper in the sample based on the amplitude of the impurity EPR spectrum in freshly prepared TlHg laccase.

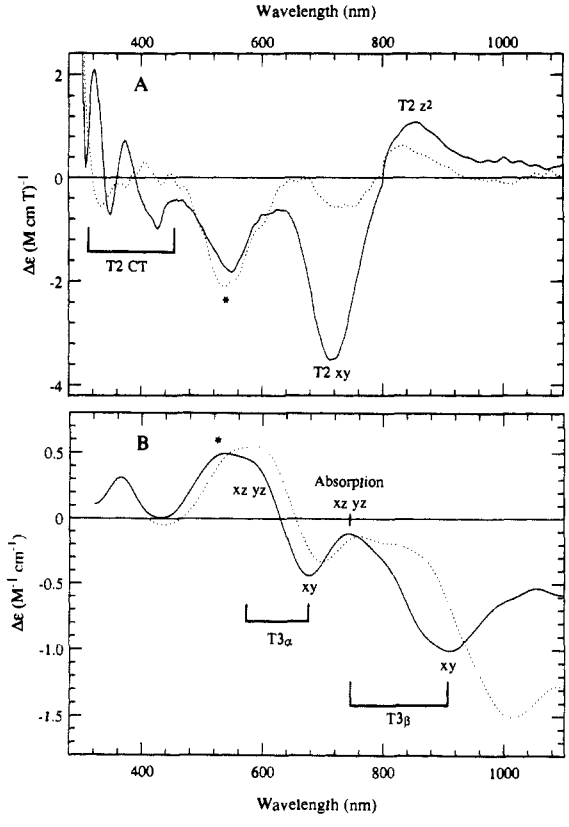

Figure 1. (A) MCD spectra of TlHg laccase at 4.2 K and 5 T. (B) CD spectra of TlHg laccase at 298 K. (—) resting enzyme; (···) resting enzyme + 10 mM F^-.

The sharp MCD features between 300 and 450 nm in Figure 1A are assigned as CT bands associated with the type 2 Cu^{2+}. Although the negative band at 426 nm may contain a contribution from a type 2 CT band, a heme impurity in the laccase preparations is known to give rise to a negative MCD feature at this wavelength,[7b] so this feature is not considered further. The intensities and energies of the three remaining CT bands do not significantly change in the pH range from 4.6 to 7.0 (data not shown). Deprotonation of a water ligand to the type 2 Cu with pK_a 6–7 has been invoked to explain changes in the type 2 Cu^{2+} EPR spectrum[6b] and the kinetics of laccase reduction.[21] The absence of a pH dependence of the three MCD features over this pH range suggests that they are not associated with bound waters, but instead with endogenous protein ligands. Two histidines have been identified as ligands to the type 2 Cu^{2+} in the crystal structure of ascorbate oxidase,[9] and N ligation to the laccase type 2 Cu^{2+} has been suggested from pulsed EPR studies of native laccase[22] and variable-frequency CW EPR studies of the TlHg derivative.[15]

(18) Byers, W.; Curzon, G.; Garbett, K.; Speyer, B. E.; Young, S. N.; Williams, R. J. P. *Biochim. Biophys. Acta* **1973**, *310*, 38–50.
(19) Press, W.; Flannery, B. P.; Teukolsky, S. A.; Vetterling, W. T. *Numerical Recipes*; Cambridge University Press: New York, 1986; pp 495–497.
(20) Lever, A. B. P. *Inorganic Electronic Spectroscopy*, 2nd ed.; Elsevier: Amsterdam, 1984; p 707.
(21) Andréasson, L.-E.; Reinhammar, B. *Biochim. Biophys. Acta* **1979**, *568*, 145–156.
(22) (a) Mondovi, B.; Graziani, M. T.; Mims, W. B.; Oltzik, R.; Peisach, J. *Biochemistry* **1977**, *16*, 4198–4202. (b) Avigliano, L.; Davis, J. L.; Graziani, M. T.; Marchesini, A.; Mims, W. B.; Mondovi, B.; Peisach, J. *FEBS Lett.* **1981**, *136*, 80–83.

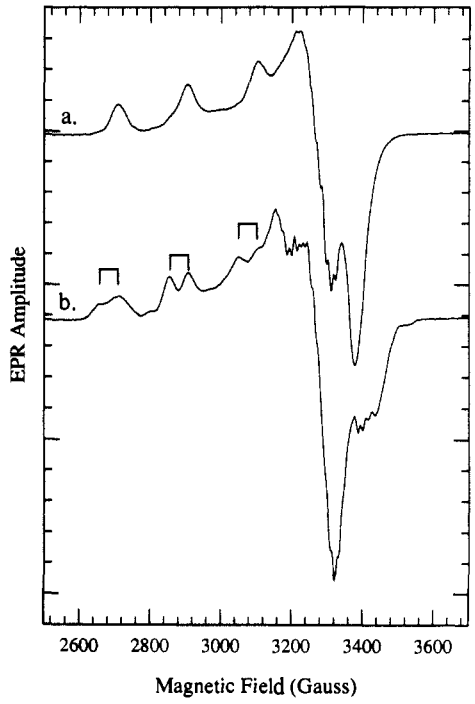

Figure 2. EPR spectra of TlHg laccase at 77 K. (a) resting enzyme; (b) resting enzyme + 10 mM F^-. The brackets indicate the $^{19}F^-$ superhyperfine coupling in the $g_{\parallel}$ region. Conditions: microwave frequency, 9.434 GHz; microwave power, 10 mW; modulation frequency, 100 kHz; modulation amplitude, 10 G; time constant, 0.2 s; sweep time, 200 s. Average of two scans.

In tetragonal imidazole–Cu^{2+} model complexes an imidazole $\pi_1 \rightarrow Cu^{2+}$ charge-transfer absorption band occurs at ~330 nm.[23] The π symmetry absorptions may be split when the imidazoles have nonequivalent orientations. The 320- and 345-nm features are both reasonably assigned as imidazole $\pi_1 \rightarrow Cu^{2+}$ charge-transfer absorption bands.

Fluoride is known to bind equatorially to the type 2 Cu^{2+} with extremely high affinity ($K > 10^4$ higher than for aqueous copper complexes).[24,25] In aqueous buffers two fluorides sequentially coordinate to the type 2 Cu^{2+},[25] but in the presence of 50% glycerol only a single fluoride binds in native laccase.[7b] Figure 2 shows the EPR spectrum of TlHg laccase in 50% glycerol–pH 6.0 phosphate buffer in the presence of a large excess of fluoride (10 mM). The well-resolved ^{19}F doublet superhyperfine splitting in the $g_{\parallel}$ region ($A_F = 54 \times 10^{-4}$ cm^{-1}) shows that a single fluoride binds equatorially to the type 2 Cu^{2+}. Fluoride binding also perturbs the electronic spectral features in TlHg laccase and these perturbations are useful in assigning the type 2 and the type 3 transitions. Upon binding fluoride, both the d → d and CT bands assigned to the type 2 Cu^{2+} show a dramatic decrease in intensity, but the contaminant band at ~550 nm is not substantially perturbed (Figure 1A). The source of intensity for the Laporté forbidden d → d transitions is the distortion-induced mixing of higher energy-allowed CT states into the pure ligand-field states. Thus, binding of F^- must perturb the CT state, which is the dominant source of intensity for the d → d transitions.

Figure 3 shows the effects of the fluoride perturbation on the 298 K absorption spectrum of TlHg laccase. In the unperturbed spectrum there is an broad shoulder at 330 nm and a weaker feature at ~620 nm. The 330-nm feature has previously been assigned as a CT band of the oxidized type 3 site.[5] However, the

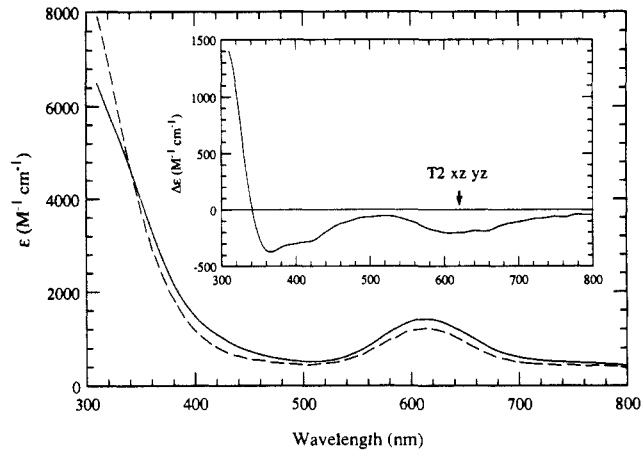

Figure 3. Absorption spectra of TlHg laccase at 277 K. (—) resting enzyme; (- - -) resting enzyme + 10 mM F^-. Inset: difference spectrum of resting enzyme + 10 mM F^- - resting enzyme.

type 2 site gives rise to MCD features in the region from 300 to 400 nm (vide supra) which will also contribute intensity to the absorption spectrum, and the 330-nm band must contain contributions from both the type 3 and type 2 sites. The TlHg laccase preparations typically have 5–10% type 1 Cu^{2+} present, and the weak band at ~620 nm contains a contribution from the residual Cys S → Cu^{2+} CT band of the type 1 Cu^{2+}. Upon addition of F^- the 330-nm band becomes sharper, showing an increase in intensity at ~310 nm and a decrease at 360 nm (see Figure 3, inset). Both the type 2 and type 3 sites are perturbed by fluoride binding (vide infra), so it is not possible to definitively assign the absorption change near 330 nm to either site. Fluoride binding also induces a decrease in the amplitude of the 620-nm absorption band (Figure 3, inset). Similar absorption changes have previously been reported in native laccase.[25] A key observation is that the amplitude of the decrease at 620 nm in TlHg laccase is similar to that observed in the native enzyme (TlHg, $\Delta\epsilon = -200 \pm 50$ M^{-1} cm^{-1}; native, $\Delta\epsilon = -210$ M^{-1} cm^{-1}). Because the amplitude does not scale with the residual amount of type 1 Cu^{2+}, this change cannot be ascribed to a perturbation of the type 1 site by fluoride, but instead it must represent a decrease in amplitude of a d → d band of the type 2 or type 3 coppers. Fluoride binding causes the type 2 d → d bands detected in MCD to decrease in amplitude (Figure 1A); in contrast, the type 3 d → d bands detected in 298 K CD spectra shift to lower energy but do not decrease in amplitude (vide infra). Therefore, the fluoride perturbation indicates that a type 2 d → d band contributes absorption intensity at 620 nm. Note that a type 3 d → d absorption band has previously been assigned in type 2 depleted (T2D) laccase[6a] and TlHg laccase.[6b] This type 3 band peaks at 740–745 nm, and clearly it is not the same feature as the type 2 band at 620 nm. The type 3 band is not observed in the TlHg laccase absorption spectrum in Figure 3 because of overlap with the residual type 1 feature at 614 nm. In summary, three type 2 d → d features have been identified: two bands at 860 (11 600 cm^{-1}) and 720 nm (13 900 cm^{-1}) are observed in the MCD spectrum and an absorption feature at 620 nm (16 100 cm^{-1}) is detected when the fluoride binding perturbation is used.

The energies of the TlHg laccase type 2 d → d features provide insight into ligand stereochemistry and electronic structure. In tetragonal five- and six-coordinate Cu^{2+} complexes with N ligands, the d → d absorption features occur at energies between 13 400 and 17 500 cm^{-1},[26] and in square-planar Cu^{2+} amino acid complexes, the transitions occur in the range from 15 400 to 17 700 and 17 500 to 20 600 cm^{-1}.[27] In contrast, the d → d bands in

(23) (a) Fawcett, T. G.; Benarducci, E. E.; Krogh-Jespersen, K.; Schugar, H. J. *J. Am. Chem. Soc.* **1980**, *102*, 2598–2604. (b) Benarducci, E.; Schwindinger, W. F.; Hughey, J. L.; Krogh-Jespersen, K.; Schugar, H. J. *J. Am. Chem. Soc.* **1981**, *103*, 1686–1691.

(24) Winkler, M. E.; Spira, D. J.; LuBien, C. D.; Thamann, T. J.; Solomon, E. I. *Biochem. Biophys. Res. Commun.* **1982**, *107*, 727–734.

(25) Brändén, R.; Malmström, B. G.; Vänngård, T. *Eur. J. Biochem.* **1973**, *36*, 195–200.

(26) (a) Hathaway, B. G.; Tomlinson, A. A. G. *Coord. Chem. Rev.* **1970**, *5*, 1–43. (b) Hathaway, B. G.; Billing, D. E. *Coord. Chem. Rev.* **1970**, *5*, 143–207.

(27) (a) Freeman, H. C. In *The Biochemistry of Copper*; Peisach, J., Aisen, P. Blumberg, W. E., Eds.; Academic Press: New York, 1966. (b) Byce, G. F. *J. Phys. Chem.* **1966**, *70*, 3549.

Table I. Ligand-Field Transitions of the Type 2-Type 3 Trinuclear Site (cm^{-1})

copper site	$d_{xz,yz} \rightarrow d_{x^2-y^2}$	$d_{xy} \rightarrow d_{x^2-y^2}$	$d_{z^2} \rightarrow d_{x^2-y^2}$
type 2	16100	13900	11600
type 3_α	17100	14800	not obsd
type 3_β	13400	11100	not obsd

the flattened tetrahedral type 1 Cu^{2+} site in plastocyanin are at much lower energies, ranging from 13900 to 5000 cm^{-1}.[4] The type 2 bands are all in the range from 16100 to 11600 cm^{-1}, indicating that this site has a five- or six-coordinate tetragonal geometry. In the EPR spectrum of the type 2 Cu^{2+} $g_z > g_{x,y} > 2$, indicating a $d_{x^2-y^2}$ ground state. In tetragonal Cu^{2+} complexes the highest energy and most intense ligand-field absorption band is the $d_{xz,yz} \rightarrow d_{x^2-y^2}$ transition.[26] The dominant type 2 d → d absorption band at 620 nm is also the highest energy transition, and it is assigned as $d_{xz,yz} \rightarrow d_{x^2-y^2}$ (Figure 3). The two remaining d → d bands, which are revealed in the MCD spectrum (Figure 1A), correspond to the $d_{z^2} \rightarrow d_{x^2-y^2}$ and $d_{xy} \rightarrow d_{x^2-y^2}$ transitions. In tetragonal Cu^{2+} systems the former transition is expected to give rise to a positive *C* term whereas the latter is expected to give a negative *C* term.[28] Therefore, the 860-nm band is assigned as $d_{z^2} \rightarrow d_{x^2-y^2}$ and the 720-nm band as $d_{xy} \rightarrow d_{x^2-y^2}$. These assignments are summarized in Table I. Note that the most intense absorption band at 620 nm does not give rise to measurable *C*-term MCD intensity. A similar observation has been made in MCD studies of the tetragonal cupric site in half-met-NO_2^- hemocyanin.[28] It was shown that the two spin–orbit components of the $d_{xz,yz} \rightarrow d_{x^2-y^2}$ transition are expected to have opposite signed *C* terms and thus give rise to a derivative-shaped pseudo-*A* term MCD signal. However, the large line widths of the two components relative to the splitting between them may reduce the intensity of the pseudo-*A* term such that it is not observed.

Electronic Spectroscopy of the Trinuclear Site: Type 3 Features. In the 298 K CD spectrum of TlHg laccase there are bands at (−)900 and (−)675 nm and a broad positive feature at 500–600 nm (Figure 1B). Based on their energies, these features are assigned as Cu^{2+} d → d transitions. Gaussian resolution of the broad feature reveals that it contains two overlapping bands centered at ~585 and 525 nm. The 525-nm band corresponds to the contaminant observed in the MCD spectrum, but the 900-, 675-, and 585-nm bands do not have corresponding MCD intensity (compare Figure 1A and B). Therefore, these features are associated with a diamagnetic ground state and they are assigned to the type 3 site. Upon binding fluoride, the 900-nm band shifts down to 1020 nm, the 675-nm band shifts to 695 nm, and the 585-nm band shifts to ~610 nm, but there is no substantial decrease in the intensity of these features. The fluoride perturbation causes the 298 K CD features to shift to lower energy, whereas fluoride binding causes the type 2 MCD and absorption bands to decrease in amplitude. This behavior confirms that the 298 K CD features are not associated with the type 2 site but with the type 3 coppers.[29]

In previous CD studies of native laccase, several features in the range from 400 to 1700 nm were observed, and it was suggested that the type 1 Cu^{2+} dominates the CD spectra of the multicopper oxidases.[30] However, the CD spectrum in Figure 1B has been corrected for the residual amount of type 1 Cu^{2+} by subtraction of an appropriately weighted native laccase CD spectrum. In addition, a control experiment demonstrates that the CD features observed in TlHg laccase do not arise from the residual 5–10% type 1 Cu^{2+}. Upon anaerobic addition of ascorbate to TlHg laccase, the bulk of the optical absorbance at 614 nm, attributed to residual type 1 Cu, bleaches immediately, indicating that the type 1 Cu^{2+} is readily reducible in the ~5–10% of the molecules that contain copper in the type 1 binding site. However, the slower decrease in the 330-nm absorption shoulder indicates that the type 3 site in TlHg laccase is reduced much more slowly, with a $t_{1/2}$ ~ 1 h.[6b] Figure 4 shows the CD spectra of anaerobic TlHg laccase before and immediately after addition of four protein equivalents of ascorbate (the type 1 Cu^{2+} spectrum has not been subtracted). The bands at 900 and 675 nm are unchanged by the reduction of the type 1 site, whereas the CD intensity between 500 and 600 nm is decreased by ~50%. The decrease in CD amplitude at 500–600 nm may be associated with reduction of the residual type 1 copper. However, the 585-, 675-, and 900-nm bands remain even after complete reduction of the residual type 1 Cu^{2+}, indicating that they indeed arise from the type 3 site and not the type 1 site. It has been observed that in TlHg laccase the type 2 site is reduced more rapidly by ascorbate than is the type 3 site,[6b] and 77 K EPR spectra of the same samples used for the ascorbate reduction CD measurements above indicate that ~2/3 of the type 2 sites were reduced. Thus, the ascorbate reduction experiment also confirms that the type 2 site does not substantially contribute to the CD spectrum of TlHg laccase.

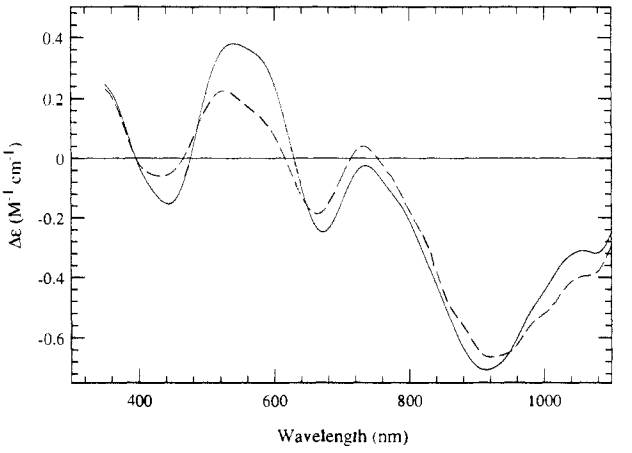

Figure 4. CD spectra of TlHg laccase at 298 K. (—) anaerobic enzyme; (- - -) anaerobic enzyme + 4 equiv of ascorbate. [TlHg] = 0.915 mM; 0.1 M potassium phosphate (pH 6.0).

The CD spectrum of the type 3 site provides new insights into the electronic and geometric structure of the coppers. The energies of the type 3 d → d transitions in Figure 1B all fall in the range from 11100 to 17100 cm^{-1}, which is characteristic of tetragonal five- or six-coordinate geometries. CD intensity requires that the scalar product of the magnetic and electric dipole transition moments be nonzero.[31] Although this is not possible in tetragonal Cu^{2+} systems, both the $d_{xy} \rightarrow d_{x^2-y^2}$ and the $d_{xz,yz} \rightarrow d_{x^2-y^2}$ transitions are magnetic dipole allowed, and they can gain CD intensity in the lower symmetry ligand fields present in protein active sites. The former transition has the greater magnetic dipole moment, and it is expected to make the more intense contribution to the CD spectrum.[31] Assignments of the type 3 ligand field transitions must take into account the three CD bands in Figure 1B as well as a previously reported absorption band at 740–745 nm, which is indicated by a hatch mark in Figure 1B.[6] The absorption band is assigned as $d_{xz,yz} \rightarrow d_{x^2-y^2}$ because this transition dominates absorption spectra of tetragonal Cu^{2+} systems.[26] It is reasonable to assign the lowest energy CD band at ~900 nm as $d_{xy} \rightarrow d_{x^2-y^2}$ because this transition should be the most intense in CD and it should be at lower energy than the $d_{xz,yz} \rightarrow d_{x^2-y^2}$ transition for tetragonal Cu^{2+}. These assignments are not consistent with the presence of two additional type 3 ligand-field CD bands at 675 and 585 nm. These latter features do not correspond to the $d_{xz,yz} \rightarrow d_{x^2-y^2}$ absorption transition at 745 nm, and they cannot be assigned as $d_{z^2} \rightarrow d_{x^2-y^2}$ because this transition is not expected to

(28) Westmoreland, T. D.; Wilcox, D. E.; Baldwin, M. J.; Mims, W. B.; Solomon, E. I. *J. Am. Chem. Soc.* **1989**, *111*, 6106–6123.

(29) There is a positive band at 365 nm in the 298 K CD spectrum (Figure 1B), but there is no reproducible perturbation of the intensity or the energy of this band upon addition of fluoride. Therefore, it is not possible to determine if this feature arises from the type 2 or type 3 sites.

(30) Dooley, D. M.; Rawlings, J.; Dawson, J. H.; Stephens, P. J.; Andréasson, L.-E.; Malmström, B. G.; Gray, H. B. *J. Am. Chem. Soc.* **1979**, *101*, 5038–5046.

(31) Yeh, C. Y.; Richardson, F. S. *Inorg. Chem.* **1976**, *15*, 682.

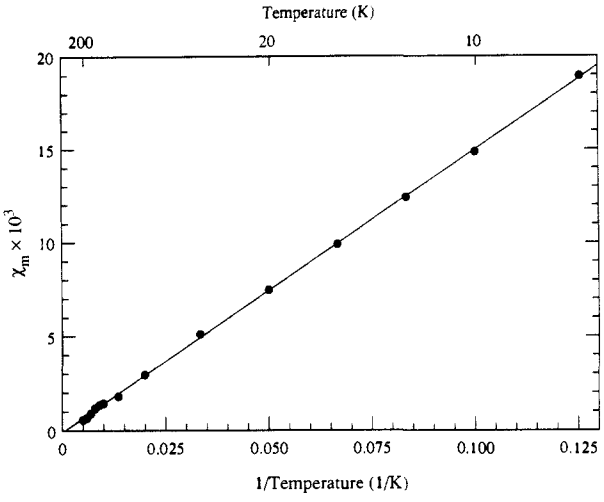

Figure 5. Magnetic susceptibility of TlHg laccase. Copper concentration, 7.60 mM. Temperature range, 8–200 K at 4 T. χ_m is expressed as susceptibility per mole of *copper*. The standard deviation of the data points is within the size of the symbols.

contribute CD intensity. However, these features may be understood by considering the observed CD spectrum in terms of a superposition of the spectra of two inequivalent type 3 coppers. The CD band at 900 nm and the absorption band at 745 nm are assigned to one copper, which for convenience is labeled type 3_β. The two CD features at 675 and 585 nm must then be assigned to the second copper, type 3_α. The energy ordering of tetragonal Cu^{2+} complexes and CD selection rules suggests that these features correspond to the $d_{xy} \rightarrow d_{x^2-y^2}$ and $d_{xz,yz} \rightarrow d_{x^2-y^2}$ transitions, respectively. The assignment of the CD spectrum in terms of two inequivalent type 3 coppers is supported by the magnitudes of the fluoride-induced energy shifts. The CD band assigned as type 3_β $d_{xy} \rightarrow d_{x^2-y^2}$ shifts $\sim$1300 cm^{-1}, whereas the type 3_α features only shift $\sim$400–500 cm^{-1} to lower energy.

We have also measured the near-IR CD of resting and fluoride-treated TlHg down to 1800 nm (data not shown). The only features observed below 1000 nm (10 000 cm^{-1}) are associated with the d $\rightarrow$ d electronic transitions of the $\sim$5% type 1 Cu^{2+} contaminant of the TlHg preparation. The assignments of the d $\rightarrow$ d electronic transitions of the type 2–type 3 trinuclear site are summarized in Table I.

Magnetic Susceptibility of the Trinuclear Site. Figure 5 shows the magnetic susceptibility of TlHg laccase from 8 to 200 K. The data show linear Curie law behavior over this entire temperature range, which corresponds to a $\mu_{eff} = 1.09\ \mu_B$ per copper. This low moment indicates that strong antiferromagnetic interactions are present, and it agrees within 1% to the moment predicted for one $S = {}^1/_2$ Cu^{2+} per trinuclear site. We have also obtained magnetic susceptibility data for met-T2D laccase, which contains an oxidized type 3 site and an oxidized type 1 site. The susceptibility for this laccase derivative shows linear Curie law behavior over the same temperature range (data not shown).

Magnetic susceptibility is a direct probe of the exchange interactions within the trinuclear site. In TlHg laccase, only one Cu^{2+} contributes to the magnetic susceptibility up to 200 K. This paramagnetism is associated with the EPR-detectable type 2 Cu^{2+}, and these data indicate that the type 3 coppers remain diamagnetic up to 200 K. Thus, antiferromagnetic coupling between the type 3 coppers is a dominant magnetic interaction within the trinuclear cluster. The possible effects of type 2–type 3 magnetic interactions will be considered below. In T2D laccase, the type 2–type 3 interactions are absent, which allows direct measurements of the antiferromagnetic coupling of the type 3 coppers. Coupling of the type 3 coppers give rise to a $S = 0$ ground state and a $S = 1$ excited state separated by $2J$. The T2D data susceptibility data give a lower limit of the singlet–triplet energy splitting of $-2J > 400$ cm^{-1}.

Azide Binding to TlHg Laccase. A series of overlapping spectral features are observed in the region from 300 to 500 nm

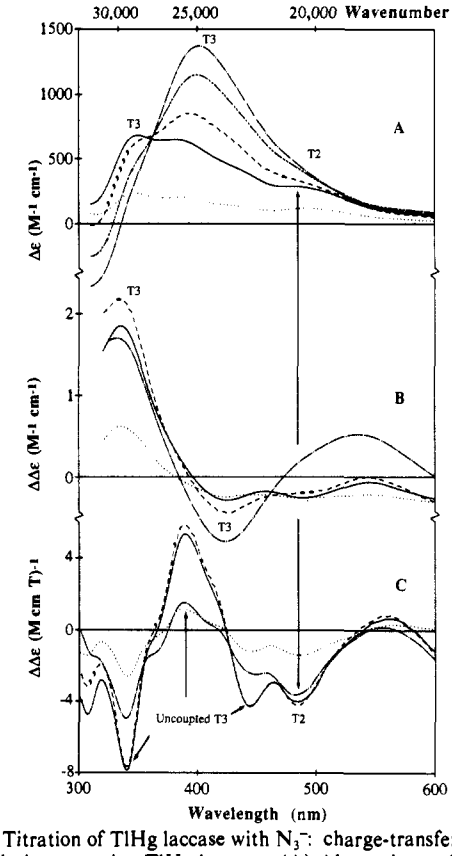

Figure 6. Titration of TlHg laccase with N_3^-: charge-transfer difference spectra relative to resting TlHg laccase. (A) Absorption at 277 K. (B) CD at 277 K. (C) MCD at 4.2 K and 5 T. (···) 0.5 mM N_3^-; (—) 2 mM N_3^-; (- - -) 5 mM N_3^-; (—··—) 10 mM N_3^-; (—·—) 20 mM N_3^-.

upon titrating TlHg laccase with azide. These features are assigned as $N_3^- \rightarrow Cu^{2+}$ charge-transfer bands (Figure 6). Because TlHg is 100% oxidized,[14] all of the azide spectral features are associated with fully oxidized sites. The azide titrations of freshly prepared TlHg laccase are extremely reproducible. However, the amplitude of the $N_3^- \rightarrow Cu^{2+}$ charge-transfer bands decreased by $\sim$50% after storage of protein at 4 °C for several weeks, and the titration behavior changed over time. Therefore, all of the azide-binding studies described herein were performed within 1 week after the TlHg laccase was prepared. In addition, all of the azide-induced features in the absorption, CD, MCD, and EPR spectra are reversible upon dialysis of the azide-bound TlHg laccase against pH 6.0 phosphate buffer.

In the absorption difference spectra a main CT band is observed at 400 nm, with shoulders at 340 and 500 nm (Figure 6A). A negative band is observed at higher energy, which is assigned to azide-induced perturbation of the type 3 absorption band at 330 nm. An isosbestic point is observed at 362 nm. The 400-nm band continues to increase over the concentration range of 0.5–20 mM azide, whereas the shoulder at 500 nm is saturated by about 2–5 mM azide, indicating that two different azide molecules coordinate to the fully oxidized trinuclear site. The equilibrium binding constants were determined from the amplitude of the Gaussian-resolved features. The 400-nm band has a binding constant of 270 ± 60 M^{-1} and the 500-nm band has a binding constant of 780 ± 200 M^{-1}. In previous studies of azide binding to native laccase, the binding constant was determined to be $\sim$200 M^{-1} for the molecules containing oxidized type 3 sites (low affinity), whereas the 22% of the sites containing reduced type 3 sites gave rise to high-affinity azide binding with $K > 10\,000$ M^{-1}.[24,32] In TlHg laccase, the lack of high-affinity azide binding associated with reduced type 3 sites allows us to resolve two binding constants associated with fully oxidized sites. The binding constant of the

(32) Morpurgo, L.; Rotillio, G.; Finazzi-Agrò, A.; Mondovi, B. *Biochim. Biophys. Acta* **1974**, *336*, 324–328.

400-nm band in TlHg laccase agrees well with the binding constant of ~200 M^{-1} previously determined for low-affinity azide binding in native laccase.[24,32] We will refer below to the azide that binds with K_1 = 780 M^{-1} as the *first azide*, and the azide that binds with K_2 = 270 M^{-1} as the *second azide*.

The concentration dependence of the absorption band at 340 nm is difficult to interpret due to interference from the loss of the higher energy type 3 absorbance feature centered at 330 nm (Figure 6A). It is clear that the 340-nm band does not represent a perturbed form of the type 3 absorbance feature at 330 nm, since the latter maximizes at ~2 mM azide, a concentration at which the loss of the type 3 feature is not yet evident. The 340-nm band is more easily monitored in the CD spectrum, where the 330-nm band does not make a significant contribution (Figure 6B). A CD band at ~355 nm corresponds to the same electronic transition observed in the absorption spectrum (Kuhn anisotropy factor $\gamma \sim 3.8 \times 10^{-3}$). This CD band is observed to saturate at ~5 mM, decreasing slightly at 20 mM. This concentration dependence is similar to that observed for the 500-nm absorption band, and these two features are both associated with the first azide.

In order to correlate the absorption spectra recorded at 277 K to the low-temperature MCD and EPR data, the azide absorption titrations were also performed in samples cooled to 77 K. The peak maxima in the $N_3^- \rightarrow Cu^{2+}$ CT bands shifted ~10–15 nm to higher energy at 77 K. However, there was no substantial difference in the binding constants for the first and second azides at the two temperatures.

In the low-temperature MCD spectra there are series of sharp features at −340, +385, −440, and −485 nm (Figure 6C). The 485-nm MCD band exhibits a similar concentration dependence to the 500-nm absorption shoulder, indicating that these features arise from the same electronic transition associated with the first azide. This transition must be associated with a paramagnetic ground state because it is observed in the low-temperature MCD spectrum, and it is assigned as first $N_3^- \rightarrow$ type 2 Cu^{2+} CT. The MCD bands at −340, +385, and −440 nm show a more complicated behavior: they increase in amplitude in parallel with the first azide spectral features up to ~2 mM, but at 20 mM all three bands decrease dramatically in intensity. Thus, no straightforward correlation exists between the absorption or CD features at 340 and 400 nm and the low-temperature MCD features, indicating that most of the intensity associated with both the 340- and 400-nm absorption/CD features is derived from a diamagnetic ground state, i.e., the type 3 site. These bands are associated with the first and second azides, respectively; the 340-nm absorption/CD band is assigned as first $N_3^- \rightarrow$ type 3 CT and the 400-nm absorption band is assigned as second $N_3^- \rightarrow$ type 3 CT. In contrast, the MCD bands at −340, +385, and −440 nm are associated with a species with a paramagnetic ground state that exhibits a different concentration dependence from the first $N_3^- \rightarrow$ type 2 Cu MCD band at 485 nm.

In addition to the electronic spectral features, a new liquid helium temperature EPR signal develops upon addition of azide to TlHg laccase (Figure 7). This broad signal is similar to one we have previously observed in native[7] and T2D laccase,[13] exhibiting a high-field turning point at g = 1.86. Thus, this signal is not directly associated with the presence of the type 2 or type 1 coppers. Owing to the absence of the type 1 Cu in TlHg laccase, the low-field part of the spectrum is also observable at g = 2.33, and at least seven Cu hyperfine lines are visible on the low-field peak, indicating that more than one Cu is contributing to the signal. The line shape, temperature dependence, and microwave saturation behavior of this signal are characteristic of the S = 1 state of a pair of dipolar coupled Cu^{2+} ions.[33] This signal is extremely similar to the EPR signals produced by protonative displacement of the endogenous bridge by azide in the coupled binuclear copper site in hemocyanin.[34] On the basis of this strong analogy, we have assigned the broad He temperature EPR signal

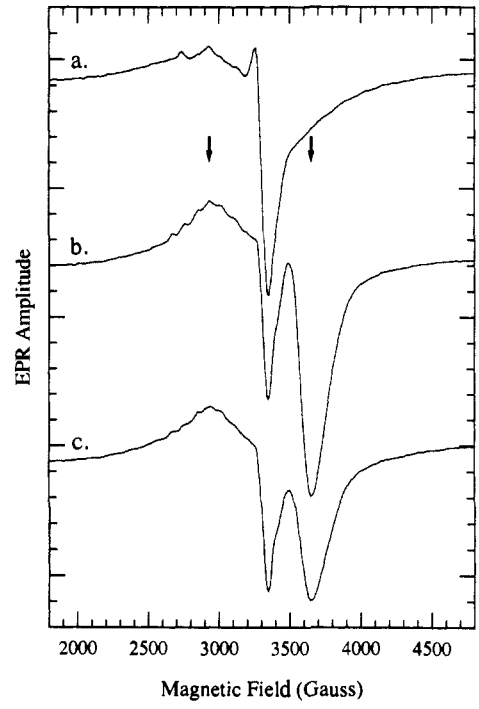

Figure 7. EPR spectra of TlHg laccase at 5 K. (a) resting TlHg laccase. (b) 5 mM N_3^-. (c) 20 mM N_3^-. Conditions: microwave frequency, 9.521 GHz; microwave power, 200 mW; modulation frequency, 100 kHz; modulation amplitude, 25 G; time constant, 0.5 s; sweep time, 500 s.

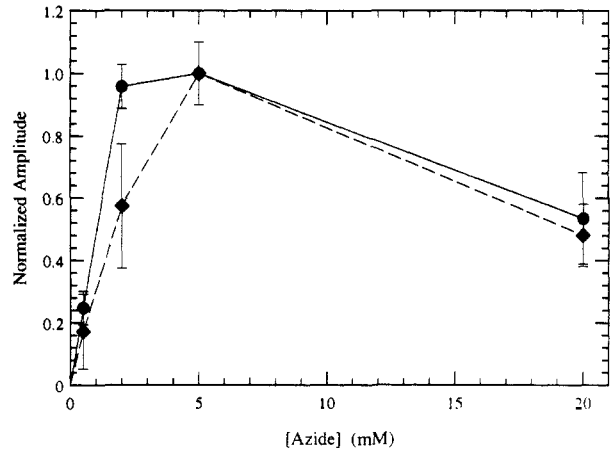

Figure 8. Amplitudes of 340, 385, and 440 nm MCD and g = 1.86 EPR vs N_3^- concentration, normalized to the amplitudes of the spectra at 5 mM N_3^-. (●) average of 340, 385, and 440 nm MCD (4.2 K, 5 T); (◆), g = 1.86 EPR signal (5 K, 200 mW). The graph represent the average of four experiments. Error bars correspond to ±1 standard deviation.

in laccase to a fraction of type 3 sites in which N_3^- and H^+ have competitively displaced and protonated the endogenous bridge, thereby disrupting the antiferromagnetic exchange interaction between the type 3 coppers and rendering them paramagnetic.[7,13] The paramagnetism of the uncoupled type 3 site means that in principle these sites contribute C-term MCD intensity. Figure 8 shows that the concentration dependence of the uncoupled EPR signal quantitatively correlates with the MCD features at 340, 385, and 440 nm; therefore, these MCD features are all assigned as $N_3^- \rightarrow$ uncoupled type 3 CT transitions. The uncoupled EPR signal has been quantitated under conditions where it is not saturated (13 K, 50 mW). The maximum increase in the double-integrated signal intensity upon addition of N_3^- corresponds to ≤10% of the type 3 sites uncoupling. Thus, only a small fraction of the type 3 sites uncouple upon binding the first N_3^-. The binding of a second lower affinity azide, as indicated by the 400-nm absorption CT band, is associated with the decrease of the uncoupled features. The maximum fraction of enzyme molecules

(33) Smith, T. D.; Pilbrow, J. R. *Coord. Chem. Rev.* **1974**, *13*, 173–278.
(34) Wilcox, D. E.; Long, J. R.; Solomon, E. I. *J. Am. Chem. Soc.* **1984**, *106*, 2186–2194.

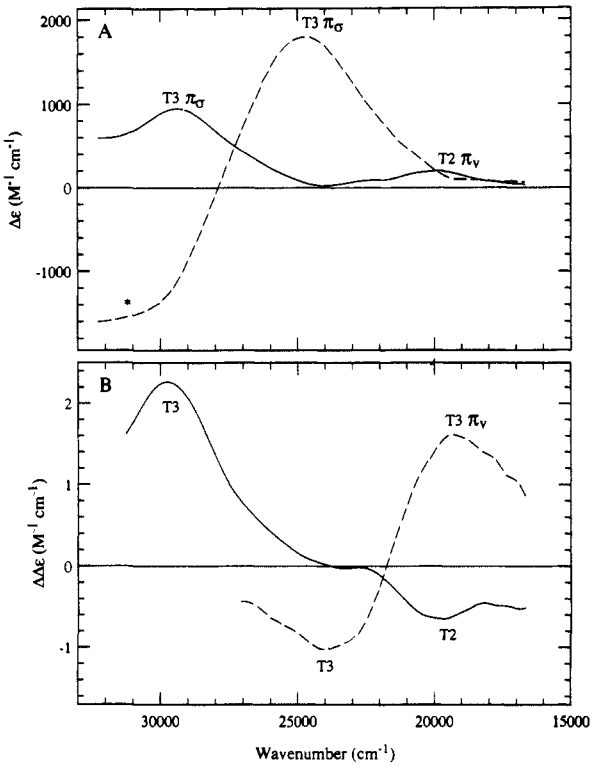

Figure 9. Spectra of the first and second azides. (A) 277 K absorption. (B) 277 K CD. (—) first N_3^-; (---) second N_3^-. The spectra of the first and second azides were obtained by subtracting the appropriately normalized spectra at 2 mM N_3^- and at 20 mM N_3^- in Figure 6, using binding constants for the first and second azides of 270 and 780 M^{-1}.

with only the first azide bound should occur at an azide concentration of $1/(K_1K_2)^{1/2}$, where K_1 and K_2 refer to the equilibrium binding constants for the first and second azides. By use of the experimental binding constants, this equation correctly predicts a maximum in the uncoupled spectral features at an azide concentration of ~2 mM. The loss of the uncoupled features could come about either by recoupling the uncoupled sites, thus rendering the sites diamagnetic, or by shifting the uncoupled signals into another spectral region. Ligand-field data presented below strongly argue for the former alternative.

The charge-transfer spectra of the first and second azides directly probe the bonding of these exogenous ligands to the trinuclear site. The highest occupied azide orbitals are a degenerate set of nonbonding π orbitals that split in energy upon bonding to Cu^{2+}.[35] One orbital (π_σ) forms a σ bond with the copper $d_{x^2-y^2}$ orbital and is strongly stabilized and the other orbital (π_v) is perpendicular to the $d_{x^2-y^2}$ plane and forms a weaker π bond to the Cu^{2+}. In terminal Cu^{2+} azide complexes, the N_3^- $\pi_\sigma \rightarrow Cu^{2+}$ CT band occurs at ~400 nm with $\epsilon \sim 2000$ M^{-1} cm^{-1}. The N_3^- $\pi_v \rightarrow Cu^{2+}$ band is not usually observed in absorption due to poor overlap with the $d_{x^2-y^2}$ orbital; however, this transition has significant magnetic dipole character and gives rise to CD features at ~500 nm in proteins or other optically active systems. In either μ-1,1 or μ-1,3 bridging geometries the π_σ and the π_v transitions split, giving rise to four possible CT transitions.

The absorption and CD spectra in Figure 6 contain overlapping spectral contributions from the first and second azides. The binding constants of these ligands are sufficiently different that the titration data in Figure 6 may be used obtain the individual absorption and CD spectra corresponding to the first and second azides (Figure 9). The first azide gives rise to two CT transitions that are active in both absorption and CD (Figure 9, solid). The MCD data in Figure 6 indicate that the low-energy feature (500 nm, 20000 cm^{-1}) is paramagnetic (type 2) and it is assigned as first N_3^- $\pi_v \rightarrow$ type 2 CT. The higher energy band (340 nm, 29500 cm^{-1}) is diamagnetic (type 3) and is assigned as first N_3^- $\pi_\sigma \rightarrow$ coupled type 3 CT. Because ≤10% of the type 3 sites uncouple, the absorption contribution of these sites to the band at 340 nm is estimated to be less than 200 M^{-1} cm^{-1}, and most of the intensity in Figure 9A is associated with the >90% coupled type 3 sites. It is noteworthy that CT features associated with both the type 2 and the type 3 sites are observed upon binding of the first azide. There are two alternative explanations for this effect: either a single azide bridges the type 2 and type 3 sites, or two different azides, both with binding constants of near 780 M^{-1}, independently coordinate as terminal ligands to the type 2 and type 3 sites. On the basis of pH dependence and azide/fluoride competition studies of native laccase,[7b] we have previously argued that this azide bridges the type 2 and type 3 sites. In the present study, the spectroscopic evidence also strongly supports this assignment. First, the 340- and 500-nm bands correspond to π_σ and π_v transitions. If each band arose from a different azide, it would require that the azide giving rise to the π_v band does not contribute any π_σ intensity in absorption. However, overlap arguments indicate that the π_σ band should be the most intense. Second, in all model complexes and protein systems with a terminal azide bound to Cu^{2+} that have been examined, the π_v band has not been detected in absorption.[35] This band is observed in the absorption spectrum of met azide Limulus hemocyanin, where azide bridges the binuclear copper site in a μ-1,3 geometry. This feature gains intensity through mixing of the π_σ and π_v orbitals induced by distortion of the coordinated azide.[35] Similarly, the N_3^- $\pi_v \rightarrow$ type 2 feature in the absorption spectrum of T1Hg laccase requires this azide strongly interacts with another site, and the most reasonable origin for this interaction is the type 3 site.

The spectral features associated with the second azide (Figure 9, dotted line) are a transition at ~405 nm (24500 cm^{-1}), which gives rise to absorption and CD, and a CD band at ~525 nm (19000 cm^{-1}). As noted above, the 405-nm band is diamagnetic, and it is assigned as second N_3^- $\pi_\sigma \rightarrow$ coupled type 3 CT. The 525-nm CD band does not give rise to a corresponding MCD feature in Figure 6C, indicating that it is also associated with the coupled type 3 site. On the basis of the low energy, it is assigned as second N_3^- $\pi_v \rightarrow$ coupled type 3 CT. The two CT bands associated with the second azide indicate that it directly coordinates the type 3 site. The amplitude of the 405-nm band ($\Delta\epsilon \sim 1800$ M^{-1} cm^{-1}) is typical of N_3^- $\pi_\sigma \rightarrow Cu^{2+}$ CT bands, indicating that the second azide binding occurs in a majority of the trinuclear centers. The uncoupled features decrease upon binding of the second azide (Figure 8), indicating that the second azide must bind to both the >90% coupled type 3 sites and to the <10% uncoupled type 3 sites.

Further insights into the mechanism of azide binding are obtained by extending the spectral studies into the low-energy ligand-field region. Figure 10 shows the MCD and CD spectra in the region from 9000 to 20000 cm^{-1} associated with resting T1Hg and samples titrated with two different concentrations of N_3^-. At 2 mM N_3^-, the first azide binding is almost saturated but there is only a small contribution of the second azide, whereas at 20 mM N_3^-, both the first and the second azide are bound. As discussed above, two type 2 d → d transitions are observed in the MCD spectrum of resting T1Hg laccase at 13900 and 16100 cm^{-1} (Figure 10A). A series of overlapping new features develop in the same energy region upon binding of the first azide, and these features are perturbed when the second azide binds. These new features are more clearly defined by subtracting the spectrum of the resting T1Hg laccase from the spectra of the azide-bound forms (Figure 10B). In this case, it is clear that three new d → d features at 11600, 16300, and 17700 cm^{-1} develop upon binding the first azide. From the CT and EPR studies it has been demonstrated that the first azide uncouples <10% of the type 3 sites; these uncoupled type 3 sites are also expected to give rise to *C*-term MCD. These new MCD features are related to the type 3 d → d bands that we have previously defined in the CD spectrum of resting T1Hg laccase (Figure 1B), and they are assigned as the

(35) Pate, J. E.; Ross, P. K.; Thamann, T. J.; Reed, C. A.; Karlin, K. D.; Sorell, T. N.; Solomon, E. I. *J. Am. Chem. Soc.* **1989**, *111*, 5198–5209.

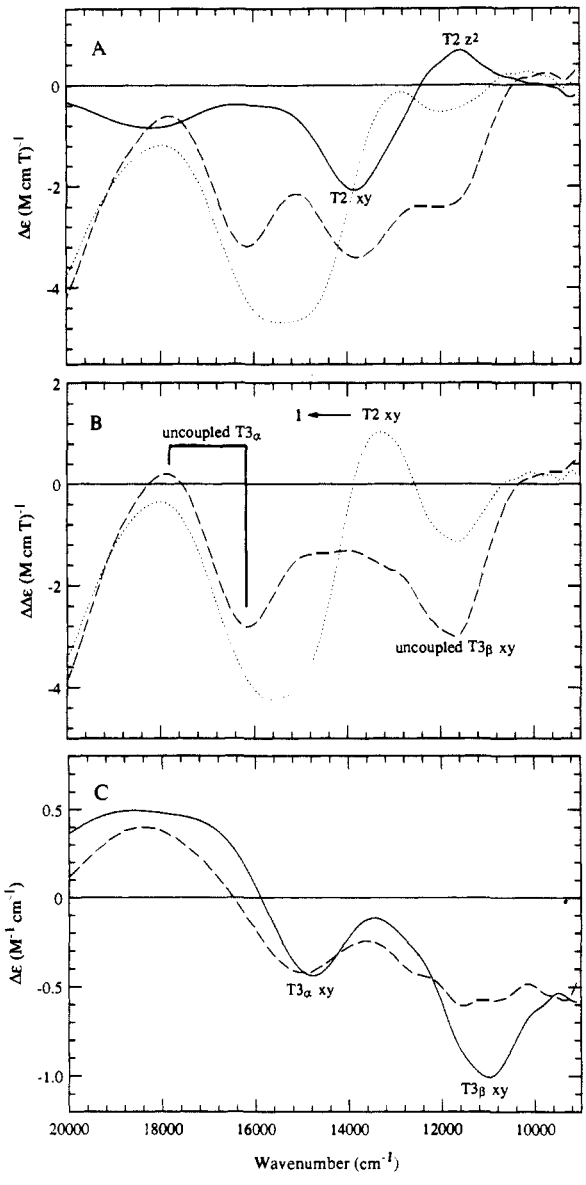

Figure 10. Titration of TlHg laccase with N_3^-: ligand-field region. (A) MCD at 4.2 K and 5 T. (—) resting enzyme; (---) 2 mM N_3^-; (···) 20 mM N_3^-. (B) MCD difference spectra relative to resting enzyme. (---) 2 mM N_3^-; (···) 20 mM N_3^-. (C) CD spectra at 277 K. (—) resting enzyme; (---) 2 mM N_3^-.

uncoupled type 3 d → d features.[36] However, these features are somewhat shifted in energy relative to the resting type 3 site (type 3_α $d_{xz,yz}$, +600 cm^{-1}; type 3_α d_{xy}, +1500 cm^{-1}; type 3_β d_{xy}, +400 cm^{-1}). Upon binding the second azide, the band at 11 600 cm^{-1} in Figure 10B decreases in amplitude, which supports the assignment as an uncoupled type 3 feature, and new features develop in the difference spectrum at +13 500 and −14 900 cm^{-1}. The new positive feature at 13 500 cm^{-1} in the difference spectrum in Figure 10B corresponds in energy to the negative type 2 $d_{xy} \rightarrow d_{x^2-y^2}$ MCD band in Figure 10A, and it is reasonable to assign the features at +13 500 and −14 900 cm^{-1} in the difference spectrum to a shift

(36) It is noteworthy that amplitude of the uncoupled type 3 d → d and CT MCD features are comparable to the amplitude of the type 2 features, despite the fact that only <10% of the type 3 sites uncouple. It is known that a similar N_3^--induced uncoupling process occurs in Busycon methemocyanin, and that the extent of uncoupling in this system is 10 ± 5% (pH 5.0, 0.1 M acetate buffer).[34] In met-azide hemocyanin MCD spectra recorded under the same conditions as the TlHg laccase spectra (5 T, 4.2 K), the maximum amplitude of the d_{xy} band is −8 (M cm T)$^{-1}$ and the amplitude of the $N_3^- \rightarrow Cu^{2+}$ CT band at 400 nm is −14 (M cm T)$^{-1}$. (Yang, E. K.; Solomon, E. I., unpublished observations). The amplitudes of these bands are comparable to those observed in TlHg (see Figures 10B and 6C).

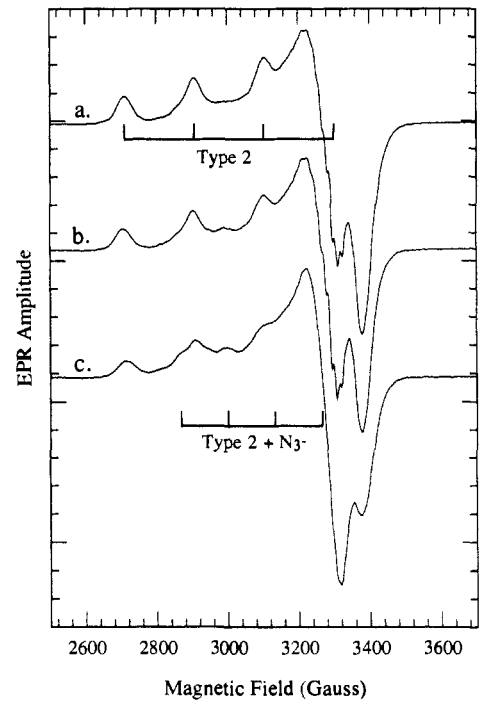

Figure 11. EPR spectra of TlHg laccase at 77 K. (a) resting enzyme; (b) +2 mM N_3^-; (c) +20 mM N_3^-. The brackets indicate the ^{65}Cu $A_\parallel$ couplings in the resting and N_3^--bound forms of the type 2 Cu^{2+}. Conditions are as in Figure 2.

in energy of the type 2 $d_{xy} \rightarrow d_{x^2-y^2}$ band of +1400 cm^{-1}. This second azide perturbation of the electronic structure of the type 2 Cu^{2+} is supported by azide-induced changes in the EPR properties of the type 2 Cu^{2+} (vide infra). The second azide MCD features associated with the type 2 perturbation occur in the same energy region as the first azide-uncoupled type 3 bands at 17 700 and 16 300 cm^{-1}. However, it is clear that the effect of second azide binding on the uncoupled type 3 d → d band at 11 600 cm^{-1} is a decrease in amplitude rather than a shift in energy, confirming that second azide binding recouples the <10% uncoupled type 3 sites.

The low-energy CD spectrum of resting TlHg laccase in Figure 10C contains the d → d bands associated with the type 3_α and the type 3_β coppers (see Figure 1B). Binding of the first azide (2 mM) causes a large decrease in the amplitude of the negative type 3_β d_{xy} band at 11 100 cm^{-1} and formation of negative intensity in the region from 12 000 to 14 000 cm^{-1} (Figure 10C, dashed line). In contrast, the type 3_α d_{xy} band at 14 800 cm^{-1} is largely unperturbed by the first azide, shifting ~+200 cm^{-1} with little or no change in amplitude. It is reasonable to correlate the formation of negative intensity in the region from 12 000 to 14 000 cm^{-1} with the loss of the type 3_β d_{xy} band at 11 100 cm^{-1}. The negative intensity cannot derive from the type 3_α d_{xy} band at 14 800 cm^{-1} since this feature is not strongly perturbed by azide. The intensity is not likely to be associated with the type 3_α feature at 17 100 cm^{-1}, since this would involve an unreasonably large energy shift of ~−4000 cm^{-1}. Thus, binding of the first azide increases the energy of the type 3_β d_{xy} band by ~+1100 cm^{-1}. However, the intensity at 12 200 cm^{-1} in the azide-perturbed spectrum is less than the intensity of the type 3_β d_{xy} band at 11 100 cm^{-1} in the resting enzyme, suggesting that binding of azide also affects the mechanism by which this feature gains significant CD intensity. No further perturbations of the type 3 d → d CD features are evident upon binding of the second azide.

Figure 11 shows the effect of first and second azide binding on the 77 K EPR of the type 2 site. The resting type 2 Cu^{2+} is characterized by a tetragonal EPR spectrum, with $g_\parallel$ = 2.245 and $A_\parallel$ = 205 × 10^{-4} cm^{-1}. At 2 mM azide (first azide) a slight decrease in the amplitude of the type 2 EPR spectrum is evident, and the spectrum of a small amount of a new tetragonal Cu^{2+} species is superimposed on the type 2 spectrum. At 20 mM azide

(second azide) there is a more substantial loss of the type 2 spectrum, and a corresponding increase in the new Cu^{2+} species. This is particularly evident in the $g_\perp$ region, where it clear that a substantial perturbation only occurs upon binding of the second azide. This new species is characterized by a smaller Cu hyperfine interaction, $A_\parallel = 140 \times 10^{-4}$ cm^{-1}, and it has previously been assigned to an azide-bound form of the type 2 Cu^{2+}.[37] The concentration dependence of the conversion of the type 2 EPR spectrum indicates that it is associated with the binding of the second azide.

The CT analysis clearly demonstrates that the first azide gives rise to type 2 and type 3 CT bands, and thus bridges the type 2 and type 3 sites, and perturbations of the d → d bands provide additional insights into the nature of azide coordination. Binding of the first azide strongly perturbs the energy of the type 3_β $d_{xy} \rightarrow d_{x^2-y^2}$ band in CD spectrum 10C, whereas the type 3_α $d_{xy} \rightarrow d_{x^2-y^2}$ band is largely unaffected. Direct binding of an exogenous ligands to an open coordination site in a metalloprotein would be expected to change the ligand-field strength and possibly to perturb the geometry of the active site, both of which could affect the energies of the d → d bands. The ligand-field strength of N_3^- is less than water or hydroxide, yet binding of the first azide results in an increase in the d → d transition energies for the type 3 coppers, indicating that the dominant effect is first azide-induced geometric distortions of the type 3_α and type 3_β coppers. The type 3_β copper is much more strongly perturbed than the type 3_α copper (ΔE = +1100 vs +200 cm^{-1}), and this suggests that the azide directly coordinates to the type 3_β but not the type 3_α copper. Thus, the first azide coordinates to the trinuclear site in an asymmetric manner, binding as a bridging ligand between the type 2 and type 3_β coppers.

There are characteristic features in the ligand-field region of the MCD spectra of TlHg laccase that probe the nature of the uncoupling process. The uncoupled type 3 d → d spectrum in Figure 10B is similar to the CD spectrum of the resting type 3 site in Figure 1B. This similarity confirms that a fraction of the type 3 sites becomes uncoupled upon binding the first azide and supports the assignment of the MCD CT bands at −340, +385, and −440 nm and the liquid helium temperature EPR signal to the uncoupled type 3 site. The uncoupled type 3 d → d bands decrease in amplitude when the second azide binds, and parallel changes are observed in the CT and EPR features. The loss of these paramagnetic features clearly demonstrates that the <10% uncoupled type 3 sites revert to a diamagnetic ground state upon binding of the second azide.

The CT spectral features of the second azide do not provide evidence for interaction with the type 2 Cu^{2+}, i.e., there are no paramagnetic CT bands, but the MCD ligand-field spectra and 77 K EPR clearly show that the electronic structure of the type 2 is perturbed upon binding this azide to the type 3 site. The magnitude and direction of the energy shift in the type 2 $d_{xy} \rightarrow d_{x^2-y^2}$ transition (+1400 cm^{-1}, Figure 10B) is comparable to that observed upon direct ligation of the first azide to the type 3_β copper (+1100 cm^{-1}). This observation suggests that the second azide also binds as bridging ligand between the type 2 and type 3 sites. The absence of any second azide → type 2 CT bands indicates weak overlap between N_3^- π and type 2 Cu^{2+} $d_{x^2-y^2}$ orbitals. In a tetragonal Cu^{2+} model system, binding of azide to an axial coordination position perturbs the d → d spectrum, but no azide → Cu^{2+} CT bands are observed.[38] Thus, the second azide may coordinate axially to the type 2 site.

We have examined the temperature dependence of the type 2 EPR and the azide → Cu^{2+} MCD CT bands in order to probe the effects of the bridged binding of the first and second azides on the magnetic interactions between the type 2 and type 3 centers. These spectral features exhibit a Curie law $1/T$ temperature dependence up to 210 K.

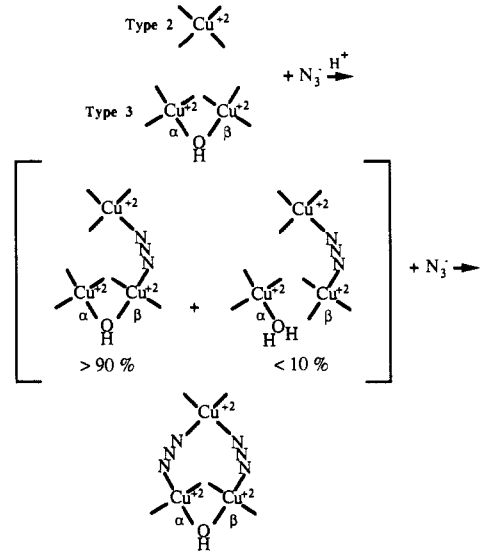

Figure 12. Spectroscopically effective model for the laccase trinuclear site.

Discussion

Resting Trinuclear Site. The application of electronic spectroscopy to the trinuclear copper site in TlHg laccase has provided new insights into the geometric and electronic structure of the Cu^{2+} centers. The electronic spectra of the three coppers have been defined by using several spectroscopies with different selection rules to separate out the type 2 and type 3 contributions, and by using the TlHg laccase derivative in which the intensely absorbing type 1 Cu^{2+} is replaced with the spectroscopically innocent Hg^{2+}. Through the MCD and absorption spectroscopy the electronic spectrum of the paramagnetic type 2 Cu^{2+} has been revealed. Three spectral features have been assigned as the d → d transitions and their energies define a tetragonal geometry at the Cu^{2+} site. The higher energy CT features are associted with histidine ligands to the type 2 site.

CD studies of the resting and fluoride-bound forms of TlHg laccase have defined the d → d spectral features of the diamagnetic type 3 site. The energies of these features indicate that the type 3 Cu^{2+} ions also have tetragonal geometries and that the coordination environments of the two coppers are inequivalent. The antiferromagnetic coupling is mediated by a bridging ligand RO^-. Based on the strength of the type 3 coupling ($-2J > 400$ cm^{-1}), reasonable candidates for R are alkyl, phenyl, or hydroxo.[2] The crystal structure of ascorbate oxidase indicates that the bridging group is a water-derived ligand,[9] which effectively rules out alkyl and phenyl. Thus, the endogenous bridge in the type 3 site is most likely OH^-. Figure 12 shows the spectroscopically effective model for the resting trinuclear site.

A set of four His-X-His sequences, which are thought to provide the histidine ligation to the type 2 and type 3 coppers, are conserved in *Neurospora crassa* laccase, human ceruloplasmin, and zucchini ascorbate oxidase.[9b,39] Given this strong homology among three different multicopper oxidases, it is likely that the same histidine ligation set exists in *Rhus* laccase. In the crystallographic model of ascorbate oxidase there are three histidine ligands per type 3 copper, arranged in a trigonal prismatic array, and two histidines that ligate the type 2 copper.[9] Thus, the spectroscopic inequivalence of the type 3 coppers does not appear to be derived from a difference in the number or kind of protein side chains that ligate each copper, but from a difference in the water-derived ligands or in the coordination geometry of each copper (vide infra). However, the definition of the type 3 and type 2 coppers in the crystal structure is based on the assumption that the type 3 coppers are equivalent and are different from the

(37) Morpurgo, L.; Desideri, A.; Rotilio, G. *Biochem. J.* **1982**, *207*, 625–627.

(38) Himmelwright, R. S.; Eickman, N. C.; LuBien, C. D.; Solomon, E. I. *J. Am. Chem. Soc.* **1980**, *102*, 5378–5388.

(39) (a) Germann, U. A.; Lerch, K. *Proc. Natl. Acad. Sci. U.S.A.* **1986**, *83*, 8854–8858. (b) Ohkawa, J.; Okada, N.; Shinmyo, A.; Takano, M. *Proc. Natl. Acad. Sci. U.S.A.* **1989**, *86*, 1239–1243.

type 2 copper. Thus, there is a possibility that the copper identified as the type 2 site in the crystal structure may actually be one of the type 3 coppers, which would lead to a difference in the number of histidine ligands for each type 3 copper.

The spectroscopically defined coordination geometries of the type 2 and type 3 coppers in *Rhus* laccase may be compared with the crystallographic model of the trinuclear site in ascorbate oxidase. In the case of the type 2 Cu^{2+}, the crystallography has identified a planar array of four equatorial ligands consisting of two histidines, a water, and a putative μ-3 bridging water-derived ligand in the middle of the triangle formed by the type 2 and type 3 coppers.[9] Thus, if it is assumed that weakly bound axial waters are present but are not resolved in the crystal structure, the type 2 site has a five- or six-coordinate tetragonal geometry and there is good agreement with the spectroscopic data. In the ascorbate oxidase structure, the type 3 coppers are coordinated by a set of three histidines, a type 3 bridging hydroxide, and the putative μ-3 bridging water-derived ligand.[9] The type 3 site symmetry is low; however, considering the three histidines and the type 3 bridging hydroxide is clear that the coordination geometry of the coppers is much closer to a distorted tetrahedral geometry than to a tetragonal geometry. Ligand-field theory predicts that a near-tetrahedral geometry would place several of the d → d transitions at energies less than 10000 cm^{-1}, which is not consistent with the spectroscopic evidence for T1Hg laccase. Thus, it is likely that the actual geometry of the type 3 coppers is closer to the tetragonal limit. Alternatively, the geometries of the type 3 sites in ascorbate oxidase may be more tetrahedral than the corresponding type 3 coppers in laccase. Unfortunately, the ligand-field spectroscopy of the type 3 sites in ascorbate oxidase is not directly accessible, owing to the absence of a well-defined T1Hg derivative. However, the UV absorbance shoulder occurs at 330 nm in both enzymes, and the energies of the N_3^- → type 3 Cu^{2+} CT bands are close,[40] suggesting that the half-occupied $d_{x^2-y^2}$ orbital is at about the same energy in both enzymes. Thus, the coordination geometries of the type 3 sites are likely to be similar in the two enzymes.

Exogenous Ligand Interactions. Azide-binding studies on T1Hg laccase have provided a detailed picture of the interactions of the trinuclear site with exogenous ligands. The previous observation of type 2–type 3 bridged binding of N_3^- in native laccase has been confirmed with the T1Hg laccase derivative. In addition, the present studies have shown that two different N_3^- molecules coordinate to the trinuclear site with different binding constants and with different spectroscopic features. The higher binding constant, first azide binds as a μ-1,3 bridging ligand between the type 2 and the type 3_β copper (Figure 12). The significant N_3^- π_v → Cu^{2+} CT intensity of the first azide indicates mixing of the π_σ and π_v orbitals induced by distortion of the coordinated azide. This distortion may involve a deviation of the Cu–N_3^-–Cu dihedral angle from planarity or from a strong interaction with a nearby residue.

A second azide binds to type 3 site with a lower binding constant, indicating that a second open coordination site exists on the type 3 site. Steric considerations suggest that the second azide binds to the other copper, the type 3_α. This second coordination site on the laccase type 3 site is not present in the coupled binuclear Cu sites in methemocyanin and mettyrosinase. In these systems, a single N_3^- bridges the binuclear site,[38,41] whereas in T2D laccase, exogenous ligands do not bridge the type 3 site.[13] The inability of exogenous ligands to bridge the type 3 site indicates that the two coordination sites are not oriented in a favorable geometry for small molecule bridging. Although second azide → type 2 CT bands are not observed, the large perturbations of the type 2 d → d features and EPR parameters strongly suggest that the second azide also bridges to the type 2 site (Figure 12).

The azide-binding studies provide insights into the mechanism of binding and four-electron reduction of dioxygen. The bridged binding of azide between the type 2 and type 3 centers suggests

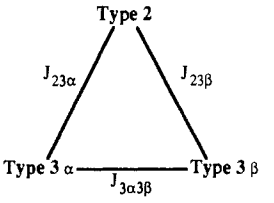

I. $|J_{3\alpha3\beta}| >> |J_{23\alpha}|, |J_{23\beta}|$
II. $J_{23\alpha} = J_{23\beta}$
III. $J_{23\alpha} = 0$
IV. $J_{23\alpha} \neq J_{23\beta} \neq J_{3\alpha3\beta}$

Figure 13. Model for the magnetic interactions within the trinuclear site.

that a similar binding mode is involved in the catalytic reduction of dioxygen. This model implies that both the type 2 and type 3 centers are required for an active catalytic site. Recently, it has been experimentally demonstrated that the type 2 Cu is required for reactivity of the trinuclear site with dioxygen.[14] We have previously noted that the type 2–type 3 bridged binding mode provides a three-electron inner-sphere electron-transfer pathway, and that concerted three-electron reduction would provide a facile route for reduction of dioxygen by irreversibly breaking the O–O bond.[7] In native laccase, it is thought that the reduction of dioxygen proceeds in two steps:[42] the first step involves concerted oxidation of the type 1 and type 3 sites, generating a three-electron-reduced oxygen intermediate, and the second step is reduction of the oxygen intermediate by the type 2 Cu, generating fully oxidized enzyme and water. It is interesting that in this model the type 2 Cu^+ is not oxidized in the primary reaction with dioxygen. Thus, the oxygen intermediate may be associated with an oxidized type 3 and a reduced type 2 site, and a role for the type 2 copper may be to stabilize this intermediate by bridging between an oxidized type 3 and a reduced type 2 copper site.

It is clear from the EPR superhyperfine couplings that fluoride directly coordinates to the type 2 Cu^{2+}, and the perturbations of the electronic features of type 3 center induced by fluoride binding suggest that it strongly interacts with both the type 2 and type 3 centers. The magnitude of the fluoride-induced perturbation of the type 3_β d_{xy} → $d_{x^2-y^2}$ CD feature is −1300 cm^{-1}, which is comparable to the shift in this feature induced by binding of the first azide (+1100 cm^{-1}). In addition, previous azide/fluoride competition experiments in native laccase have clearly shown that F^- does not bind to the type 2 Cu^{2+} in the presence of a reduced type 3 site,[7b] suggesting F^- must strongly interact with the oxidized type 3 coppers. Indeed, binding of F^- is known to lower the redox potential of the type 3 site in *Rhus* laccase from 434 to ~390 mV;[5] this decrease may arise from preferential coordination of F^- to the oxidized type 3 site. The strong interaction of fluoride with the oxidized type 3 center provides insight into the unusually high affinity of F^- for the trinuclear site ($K \sim 40000\ M^{-1}$).

Magnetic Properties of the Trinuclear Site. A spin-coupling model is the appropriate formalism to define the magnetic properties of the type 2–type 3 trinuclear site. Based on the susceptibility results, this model must include a strong antiferromagnetic coupling between the type 3 coppers. In addition, type 2–type 3 exchange interactions must also considered. In the present study it has been demonstrated that exogenous ligands are capable of bridging the type 2 and type 3 sites, and the crystallographic data on ascorbate oxidase point to a potential μ-3 bridging ligand between the three coppers.[9] Thus, in the ligand-bound forms of the trinuclear site, and possibly in the resting site, there exist type 2–type 3 bridging moieties capable of acting as superexchange pathways.

Exchange-coupled trinuclear systems have been the subject of theoretical and experimental investigations.[43,44] Below, a model

(40) Cole, J. L.; Avigliano, L.; Morpurgo, L.; Solomon, E. I., manuscript in preparation.
(41) Himmelwright, R. S.; Eickman, N. C.; LuBien, C. D.; Lerch, K.; Solomon, E. I. *J. Am. Chem. Soc.* **1980**, *102*, 7339–7344.
(42) (a) Andréasson, L.-E.; Brändén, R.; Reinhammar, B. *Biochim. Biophys. Acta* **1976**, *438*, 370–379. (b) Reinhammar, B.; Malmström, B. G. In *Copper Proteins*; Spiro, T. G., Ed.; Wiley Interscience; New York, 1981; Chapter 3.
(43) (a) Griffith, J. S. *Struct. Bonding (Berlin)* **1972**, *10*, 87–126. (b) Sinn, E. *Coordin. Chem. Rev.* **1970**, *5*, 313–347.
(44) (a) Banci, L.; Bencini, A.; Gatteschi, D. *Inorg. Chem.* **1983**, *22*, 2681–2683. (b) Banci, L.; Bencini, A.; Dei, A.; Gatteschi, D. *Inorg. Chem.* **1983**, *22*, 4018–4021. (c) Gatteschi, D.; Bencini, A. In *Magneto-Structural Correlations in Exchange Coupled Systems*; NATO ASI Series; Willett, R. D., Gatteschi, D., Kahn, O., Eds.; Reidel Publishing Co.: Dordrecht, The Netherlands, 1985; pp 241–268.

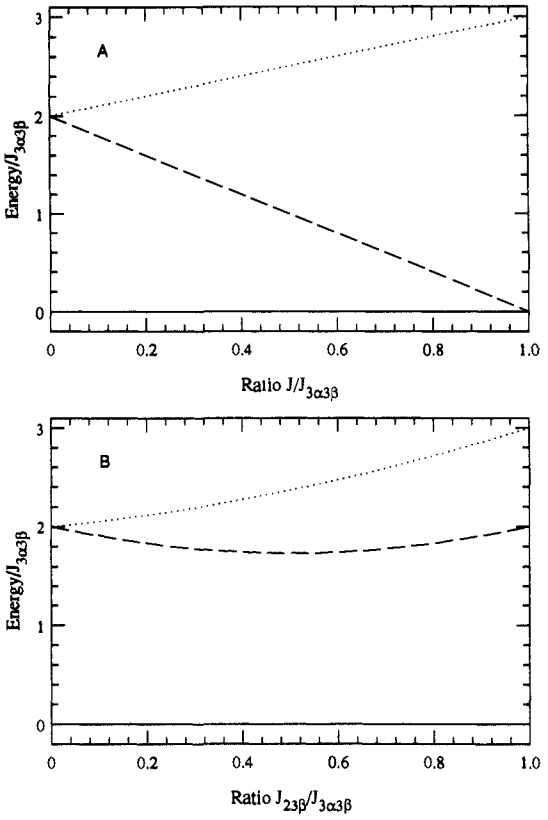

Figure 14. Energy levels for exchange-coupled Cu^{2+} trimer. (A) $J = J_{23\alpha} = J_{23\beta}$. (B) $J_{23\alpha} = 0$. (···) $|^3/_2\rangle$ state; (- - -) $|^1/_2 b\rangle$ state; (—) $|^1/_2 a\rangle$ state.

is developed that considers the implications of type 2–type 3 exchange interactions for the magnetic properties of the trinuclear copper site in the multicopper oxidases. Two kinds of effects are expected: (1) exchange coupling of the three coppers will generate excited spin states that may be probed by magnetic susceptibility measurements and by variable-temperature EPR and MCD spectroscopies and (2) the EPR and MCD spectra associated with the ground $S = {}^1/_2$ state can exhibit features from all three coppers. These effects will be considered for both the resting trinuclear site and the anion-bound forms. In order to model these various forms, the spin-coupling formalism will be used to consider isotropic exchange interactions among the three coppers in several limiting cases defined in Figure 13. Note that case I corresponds to the limit where the type 3 coupling is much greater than the type 2–type 3 interactions. This situation corresponds to the earlier models of the type 2 and type 3 sites, in which type 2 Cu^{2+} can be considered a magnetically isolated $S = {}^1/_2$ ion and the type 3 site a strongly antiferromagnetically coupled dimer with an $S_{total} = 0$ ground state. The other cases involve type 2–type 3 couplings, and more complex magnetic coupling schemes must be considered.

First, we consider the effects of type 2–type 3 interactions on the energies of the excited spin multiplets. In a symmetric trinuclear site where the couplings between each of the type 3 coppers and the type 2 copper are equivalent (case II, Figure 13) the spin Hamiltonian can be written as[43]

$$\mathbf{H} = -2J(\mathbf{S}_2\cdot\mathbf{S}_{3\alpha} + \mathbf{S}_2\cdot\mathbf{S}_{3\beta}) - 2J_{3\alpha3\beta}\,\mathbf{S}_{3\alpha}\cdot\mathbf{S}_{3\beta}$$

where J is the coupling between the type 2 and each of the type 3 coppers and $J_{3\alpha3\beta}$ is the coupling between the type 3 coppers. The three $S = {}^1/_2$ ions are coupled to give one quartet state and two doublet states labeled a and b. The quartet arises from parallel orientation of all three spins. The doublet states are defined by an intermediate quantum number $S^* = S_{3\alpha} + S_{3\beta}$; for state a, $S^* = 0$, and for state b $S^* = 1$. The energies of these states are shown in Figure 14A as a function of the ratio of the type 2–type 3 coupling J to the type 3 coupling $J_{3\alpha3\beta}$. At low J, the splitting between the doublets is $-2J_{3\alpha3\beta}$. The susceptibility measurements on met-T2D laccase demonstrate that the exchange interaction between the type 3 coppers $-2J_{3\alpha3\beta} > 400\ cm^{-1}$. As the magnitude of J increases, the splitting decreases linearly, up to the limit of $J = J_{3\alpha3\beta}$, where the doublets are degenerate. Thus, the excited doublet state becomes thermally accessible only when the type 2–type 3 coupling constants approach $-2J = 400\ cm^{-1}$. Population of this excited doublet state would be expected to give rise to new features in the MCD and EPR spectra of the trinuclear site (vide infra). However, the magnetic moment of the site will only increase upon population of the $S = {}^3/_2$ state. The minimum energy of this state is $2J_{3\alpha3\beta}$, and the splitting increases as J increases. Given the large magnitude of $J_{3\alpha3\beta}$, this state will not be thermally accessible.

For the general case where all three couplings are unequal the appropriate spin Hamiltonian is

$$\mathbf{H} = -2J_{23\alpha}\,\mathbf{S}_2\cdot\mathbf{S}_{3\alpha} - 2J_{23\beta}\mathbf{S}_2\cdot\mathbf{S}_{3\beta} - 2J_{3\alpha3\beta}\,\mathbf{S}_{3\alpha}\cdot\mathbf{S}_{3\beta}$$

In this case the doublet states are mixed, and the energies of the three states are a function of all three J couplings.[43] The energies of the three states are plotted in Figure 14B for the case where the type 2–type 3 coupling $J_{23\alpha}$ is zero (case III). The minimum splitting between the doublet states is $\sim 1.7J_{3\alpha3\beta}$ and occurs when $J_{23\beta} = {}^1/_2 J_{3\alpha3\beta}$. The minimum splitting between the ground doublet and the quartet excited state is $2J_{3\alpha3\beta}$ and occurs when $J_{23\beta}$ is zero. Thus, given a large $2J_{3\alpha3\beta}$ coupling, both the excited doublet and quartet states will not be thermally accessible in this case. For the general case where all three J's are unequal (case IV), the splitting to the quartet is again dominated by the large negative $J_{3\alpha3\beta}$. However if $J_{23\alpha}$ and $J_{23\beta}$ are comparable and approach the magnitude of $J_{3\alpha3\beta}$, the excited doublet state may become thermally accessible by the EPR and MCD measurements.

The spin Hamiltonian properties of the $|^1/_2 a\rangle$ ground state also provide insights into the exchange interactions among the three coppers.[44] The ground-state wave function for positive M_s is

$$\left|\frac{1}{2}, a\right\rangle = \left(\frac{1}{\sqrt{2}}\cos\omega + \frac{1}{\sqrt{6}}\sin\omega\right)\Big|{+}{+}{-}\rangle + \left(-\frac{1}{\sqrt{2}}\cos\omega + \frac{1}{\sqrt{6}}\sin\omega\right)\Big|{+}{-}{+}\rangle + \left(-\frac{2}{\sqrt{6}}\sin\omega\right)\Big|{-}{+}{+}\rangle \quad (1)$$

where the angle ω is defined in eq 2[45]

$$\omega = \frac{1}{2}\tan^{-1}\left[\frac{\sqrt{3}(J_{23\beta} - J_{23\alpha})}{2J_{3\alpha3\beta} - J_{23\alpha} - J_{23\beta}}\right] \quad (2)$$

and $|{+}{+}{-}\rangle$ corresponds to $M_s = +{}^1/_2$ for type 2 and 3_α coppers and $M_s = -{}^1/_2$ for the type 3_β copper, etc. The $\mathbf{g}$ tensor of this state can be expressed as a function of the $\mathbf{g}$ tensors of the individual ions[44]

$$\mathbf{g}\left(\frac{1}{2}, a\right) = c_2\mathbf{g}_2 + c_{3\alpha}\mathbf{g}_{3\alpha} + c_{3\beta}\mathbf{g}_{3\beta} \quad (3)$$

where the coefficients in eq 3 are given by

$$c_2 = \cos^2\omega - \frac{1}{3}\sin^2\omega$$
$$c_{3\alpha} = \frac{2}{3}\sin^2\omega + \frac{2}{\sqrt{3}}\sin\omega\cos\omega \quad (4)$$
$$c_{3\beta} = \frac{2}{3}\sin^2\omega - \frac{2}{\sqrt{3}}\sin\omega\cos\omega$$

The $\mathbf{g}$ tensors of the individual ions must be expressed in the coordinate system of the trinuclear site $\mathbf{g}$ tensor prior to performing the summation over the individual ions.

(45) Note that the expression for ω in ref 44 is in error.

In addition, the EPR spectra of the trimer will exhibit hyperfine couplings from the three Cu^{2+} ions, and the hyperfine tensors in the coupled system $\mathbf{A}_i$ are related to the single-ion hyperfine tensors $\mathbf{a}_i$ by

$$\langle a, b|\mathbf{A}_i\mathbf{S}|a, b\rangle = \langle a, b|\mathbf{a}_i\mathbf{S}_i|a, b\rangle \qquad i = 2, 3_\alpha, 3_\beta \quad (5)$$

where in eq 5 S refers to the coupled system and $\mathbf{S}_i$, $i = 2, 3_\alpha, 3_\beta$, are the spin operators associated with the type 2 and type 3 coppers. Thus

$$\mathbf{A}_2 = c_2\mathbf{a}_2 \qquad \mathbf{A}_{3\alpha} = c_{3\alpha}\mathbf{a}_{3\alpha} \qquad \mathbf{A}_{3\beta} = c_{3\beta}\mathbf{a}_{3\beta} \quad (6)$$

The single-ion hyperfine tensors must be projected onto the coordinate system of the trinuclear site **g** tensor. In mononuclear Cu^{2+} systems, the direction of A_z is generally close to that of g_z, so that the same transformation that relates the single-ion **g** tensors to the trimer **g** tensor also can be used to relate the single-ion hyperfine couplings to the trimer **g** tensor.

The paramagnetic *C*-term MCD behavior of a coupled trinuclear copper unit will exhibit contributions from electronic transitions centered on the three individual Cu^{2+} ions. The expression for an orientationally averaged MCD *C* term associated with a spin-degenerate ground state for an individual Cu^{2+} ion is[46]

$$C_0 = -\frac{i}{3}\sum_{\alpha\alpha'\lambda}\langle A\alpha'|(\mathbf{L} + 2\mathbf{S})|A\alpha\rangle\cdot(\langle A\alpha|\mathbf{m}|J\lambda\rangle \times \langle J\lambda|\mathbf{m}|A\alpha'\rangle) \quad (7)$$

The sum in eq 7 is over all spin components of the ground ($\alpha\alpha'$) and excited (λ) states. The function $\langle A|$ corresponds to the orbital ground state and the function $\langle J|$ corresponds to an orbital excited state. In Cu^{2+} systems with orbitally nondegenerate ground states, spin–orbit coupling is required for nonzero *C*-term MCD. In a system containing three exchange-coupled tetragonal Cu^{2+} ions, the d → d and the ligand → metal CT transitions can be considered as localized on individual Cu^{2+} ions. In general, spin–orbit coupling is a single-center operator and will only couple the spin and orbital angular momentum associated with a single atom. Therefore, in the ground doublet state of the coupled system, the Zeeman term in eq 7 results in a nonzero contribution to the *C*-term MCD only for those components of the ground doublet spin state that are associated with the same ion as the electronic transition. The *C*-term intensities in the trinuclear site are weighted by the same c_i coefficients that govern the EPR spin Hamiltonian parameters, and the *C*-term MCD associated with the $|^1/_2\ a\rangle$ state is given by

$$C_0\left(\frac{1}{2}, a\right) = c_2C_{0(2)} + c_{3\alpha}C_{0(3\alpha)} + c_{3\beta}C_{0(3\beta)} \quad (8)$$

where the $C_{0(i)}$ in eq 8 refers to the *C* terms associated with electronic transitions at each of the three coppers in the trinuclear site.

These expressions lead to clear predictions regarding the effects of the type 2–type 3 magnetic interactions on the EPR and LMTCD spectra of the laccase trinuclear copper site for the various cases listed in Figure 13. In case I $|J_{3\alpha3\beta}| \gg |J_{23\alpha}|, |J_{23\beta}|$ and the ground-state coefficients are $c_2 = 1$, $c_{3\alpha} = c_{3\beta} = 0$, reflecting an $S = {}^1/_2$ state localized on the type 2 Cu^{2+}. Interestingly, in case II the doublet wave functions do not mix, and $c_{23\alpha}$ and $c_{23\beta}$ will also equal zero regardless of the magnitude of $J_{23\alpha} = J_{23\beta}$ relative to $J_{3\alpha3\beta}$. Thus, the paramagnetism will be localized on the type 2 Cu^{2+} and the EPR and *C*-term MCD of the trinuclear site will only reflect the properties of the type 2 Cu^{2+} if $J_{23\alpha}$ and $J_{23\beta}$ are small relative to the type 3 coupling or if they are equal. Case III is illustrated in Figure 15, which shows the dependence of the ground-state coefficients on the ratio $J_{23\beta}/J_{3\alpha3\beta}$ where $J_{23\alpha} = 0$. The coefficients of the type 3 coppers $c_{3\alpha}$ and $c_{3\beta}$ diverge from 0 and c_2 decreases from 1 as $J_{23\alpha}/J_{3\alpha3\beta}$ diverges from 0 in either the positive or negative direction. Finally, consider the most general case with three unequal exchange couplings between the three coppers. Simulations indicate that the most substantial deviations are expected if the couplings of the two type 3 coppers to the type 2 copper are of opposite sign and are of comparable magnitude to the couplings between the two type 3 coppers.

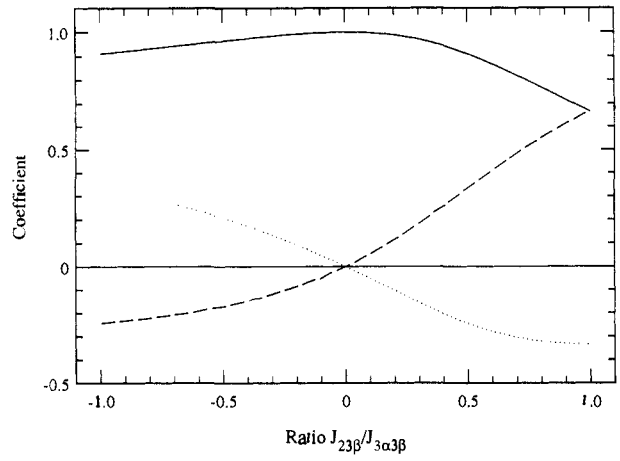

Figure 15. Dependence of EPR and MCD ground-state weighting coefficients on the exchange couplings in an Cu^{2+} trimer where $J_{23\alpha} = 0$. (—) c_2; (- - -) $c_{3\alpha}$; (···) $c_{3\beta}$.

The analysis of the energy splittings and ground-state properties may be used to estimate limits to the magnitude of the exchange couplings between the type 2 and type 3 coppers in the resting and ligand-bound forms of the trinuclear site. In the resting form, the resolved type 2 Cu^{2+} hyperfine coupling is at the upper end of the range for type 2 Cu^{2+} systems ($A_\parallel = 205 \times 10^{-4}$ cm^{-1}). This coupling will decrease as c_2 decreases from 1.0 due to nonzero exchange interaction between the type 2 and type 3 sites. Thus, a conservative lower limit on c_2 would be 0.9. In the 77 K EPR spectrum of T1Hg laccase there is no evidence for hyperfine interactions with the type 3 coppers. In addition, the type 3 d → d bands identified in the CD spectrum do not contribute measurable *C*-term MCD intensity, requiring that $c_{3\alpha}$ and $c_{3\beta}$ are close to zero. It is possible to assign reasonable limits on the magnitude of the type 3 exchange coupling. The susceptibility measurements on met-T2D laccase show that $-2J_{3\alpha3\beta} > 400$ cm^{-1}. In monohydroxo bridged Cu^{2+} dimer model systems, the exchange couplings range from $-2J = 64$ to $-2J = \sim 1000$ cm^{-1} with corresponding Cu–O–Cu angles of 110° and 144°.[47] The Cu–O–Cu angle in the crystallographically defined trinuclear site in ascorbate oxidase is ~135°.[9] Although additional geometric factors clearly are important in determining the magnitude of the exchange couplings, these considerations suggest that the value of $-2J_{3\alpha3\beta}$ is between 400 and 1000 cm^{-1}. In the absence of any bridging ligand(s) between the type 2 and type 3 centers in the resting trinuclear site, $J_{23\alpha}$ and $J_{23\alpha}$ are both close to zero (case I), and the type 2 and type 3 centers may be considered as magnetically isolated centers. Alternatively, the μ-3 water-derived ligand may provide a superexchange pathway between the type 2 and each of the type 3 coppers such that $J_{23\alpha} = J_{23\beta}$ (case II). Thus, in both cases, the ground-state properties only reflect the contribution of the type 2 Cu^{2+}, which is consistent with the experimental results. Also, within this model the large value of $J_{3\alpha3\beta}$ renders the quartet state thermally inaccessible, which is consistent with the susceptibility data on T1Hg laccase (Figure 5). However, if the type 2–type 3 couplings are comparable to $J_{3\alpha3\beta}$, then the excited doublet state may be accessible. In a trinuclear Cu^{2+} model systems containing a μ-3 OH^- bridging moiety, $-2J \sim 250$ cm^{-1}.[48] Thus, if $2J_{3\alpha3\beta}$ is close to the lower

(46) Stephens, P. J. *Adv. Chem. Phys.* **1976**, *35*, 197–264.

(47) (a) Haddad, M. S.; Wilson, S. R.; Hodgson, D. J.; Hendrickson, D. N. *J. Am. Chem. Soc.* **1981**, *103*, 384. (b) Haddad, M. S.; Hendrickson, D. N. *Inorg. Chim. Acta* **1978**, *28*, L121–L122. (c) Burk, P. L.; Osborn, J. A.; Youinou, M.-T.; Agnus, Y.; Louis, R.; Weiss, R. *J. Am. Chem. Soc.* **1981**, *103*, 1273. (d) Drew, M. G. B.; McCann, M.; Nelson, S. M. *J. Chem. Soc., Dalton. Trans.* **1981**, 1868. (e) Drew, M. G. B.; Nelson, J.; Escho, F. McKee, V.; Nelson, S. M. *Ibid.* **1982**, 1837. (f) Coughlin, P. K.; Lippard, S. J. *J. Am. Chem. Soc.* **1984**, *106*, 2328–2336.

(48) Butcher, R. J.; O'Conner, C. J.; Sinn, E. *Inorg. Chem.* **1981**, *20*, 537–545.

limit determined by the susceptibility measurements, the excited doublet state would be only ~150 cm^{-1} above the ground state. In this regard, there have been reports of temperature-dependent changes in the EPR properties of the type 2 Cu^{2+} site in laccase;[49] in particular, the value of $A_\parallel$ was observed to change as a continuous function of temperature, decreasing by ~25% upon warming from 77 K to room temperature.[49] Parallel temperature-dependent changes in the type 1 EPR properties were also observed, and these effects were ascribed to a temperature-dependent conformational change in the protein. However, an alternative explanation for the changes in the type 2 EPR properties is population of the $|^1/_2 b\rangle$ state at high temperature. This state would give rise to a complex EPR signal with hyperfine couplings associated with the type 3 coppers, since if c_2 is close to 1.0 in the ground state, then in the $|^1/_2 b\rangle$ state $c_2 \sim -^1/_3$ and $c_{3\alpha}$ and $c_{3\beta} \sim {}^2/_3$.[50] The observed high-temperature EPR spectrum could then represent a superposition of the spectra of the $|^1/_2 a\rangle$ and $|^1/_2 b\rangle$ states. There is precedent for this behavior: in an EPR study of a model trinuclear Cu^{2+} system, the g values were observed to be temperature dependent, indicating thermal population of the higher $S = {}^1/_2$ state.[44a]

The first N_3^- bridges the type 2 and the type 3_β coppers (Figure 12), and in this system it is appropriate to consider $J_{23\alpha} \sim 0$ (case III). The type 2 EPR at 77 K and the ligand-field MCD at 4.2 K are not perturbed upon binding the first azide, indicating that the coefficient c_2 remains close to 1.0. Note that the uncoupled MCD and EPR features do not reflect the bulk of the trinuclear sites, but are associated with a subpopulation of sites in which binding of the first azide displaces the type 3 endogenous bridge. If the type 2–type 3 coupling $J_{23\beta}$ is antiferromagnetic, the coefficient of the type 2 copper decreases below 0.9 and the type 3 coefficients increase above 0.1 at values of $J_{23\beta} \sim -50$ to -250 cm^{-1}. In copper dimer systems, μ-1,3 azide is capable of mediating strong antiferromagnetic coupling. In the only structurally characterized monobridged μ-1,3 copper dimer $-2J = 309$ cm^{-1}.[51] Thus, the ratio $J_{23\beta}/J_{3\alpha 3\beta}$ is expected to lie between ~0.7 and 0.3, which would result in a substantial perturbation of the ground-state wave function (Figure 15). The absence of such effects indicates that the exchange coupling mediated by first azide is substantially less than in the model system. The first azide charge-transfer spectrum (Figure 9) indicates that type 3_β $d_{x^2-y^2}$ bonds with the N_3^- π_σ orbital, whereas the type 2 $d_{x^2-y^2}$ bonds with the N_3^- π_v orbital. These azide orbitals are orthogonal; thus, there is weak overlap between magnetic orbitals on the type 2 and type 3 coppers, which would result in a substantial perturbation of the antiferromagnetic interaction expected for the μ-1,3 bridging azide.

The second azide likely bridges the type 3_α and the type 2 coppers (Figure 12); thus $J_{23\alpha}$ may be nonzero. The type 2 EPR spectrum is altered upon binding of the second azide; however, this change is associated with geometric perturbation of the type 2 site and not with a change in the spin localization within the ground state of the trinuclear site. The absence of any second $N_3^- \rightarrow$ type 2 Cu^{2+} CT intensity (Figures 6 and 9) indicates weak orbital overlap with the type 2 $d_{x^2-y^2}$ magnetic orbital. Thus, like the first azide, the second azide does not appear to mediate strong antiferromagnetic exchange between the type 2 and the type 3 coppers.

A combination of EPR and CD measurements strongly suggests that fluoride bridges the type 2 and type 3 centers. The 77 K EPR spectra indicate that $g_\parallel$ increases slightly from 2.25 to 2.28 when fluoride binds, but the type 2 Cu hyperfine interaction is not changed, suggesting there is no substantial perturbation of the $S = {}^1/_2$ ground state induced by F^- binding. The decrease in the intensity of the type 2 MCD features induced by fluoride binding is accompanied by a decrease in a ligand-field absorption feature, indicating that these effects cannot be ascribed to a decrease in c_2. No monobridged F^- Cu dimer systems have been structurally defined, but dibridged F^- mediates only moderately strong antiferromagnetic interactions ($-2J = 118$ cm^{-1}).[52] Thus, the EPR and MCD results that indicate that the ground state is not perturbed by the binding of fluoride are compatible with the moderate exchange interactions expected to result from F^- bridging the type 2 and type 3 sites. Interestingly, the fluoride superhyperfine couplings in the 77 K EPR spectra of the type 2 Cu^{2+} are not observed at 298 K,[49b] but azide/fluoride competition studies clearly demonstrate that fluoride does bind at 298 K.[7] The absence of fluoride hyperfine couplings in the 298 K EPR spectra may be associated with population of the $|^1/_2 b\rangle$ state. As in the case of the resting trinuclear site, the $|^1/_2 b\rangle$ state in the fluoride derivative will be delocalized over the three coppers of the trinuclear site. This delocalization will have the effect of reducing the fluoride superhyperfine coupling to the type 2 Cu^{2+} such that it is not detectable at 298 K.

The spin-coupling model provides a useful context to understand the magnetic behavior of the resting and ligand-bound forms of the trinuclear site. In general, this model suggests that the effects of type 2–type 3 magnetic interactions are difficult to detect because of the strong antiferromagnetic coupling between the type 3 coppers ($-2J_{3\alpha 3\beta} > 400$ cm^{-1}). In all of the coupling schemes depicted in Figure 15, the energy of the $|^3/_2\rangle$ state is at least $2J_{3\alpha,3\beta}$ above the ground state, so that *magnetic susceptibility measurements will only show deviations from Curie behavior in derivatives in which the magnitude of the type 3 coupling is reduced by perturbation of the endogenous bridge.* In the case where $J_{23\alpha} = J_{23\beta}$, the $|^1/_2 a\rangle$ ground state is localized on the type 2 Cu^{2+} and the type 2–type 3 coupling will have no effect on the low-temperature EPR and MCD spectra. If the type 2–type 3 coupling is comparable to $J_{3\alpha 3\beta}$, the energy of the $|^1/_2 b\rangle$ state decreases, i.e., the trinuclear site becomes spin frustrated, and variable-temperature EPR and MCD measurements are useful probes of the type 2–type 3 site interactions. The interpretation of the variable-temperature EPR measurements is complicated by possible temperature-dependent conformational changes;[49] however, population of the $|^1/_2 b\rangle$ state may be unambiguously detected by probing for possible paramagnetic MCD features associated with type 3 site. In contrast, if one of the type 2–type 3 couplings is zero, then the $|^1/_2 b\rangle$ state is not thermally accessible, but the ground-state wave function becomes delocalized over the three coppers, and the EPR and MCD spectra will contain contributions from both the type 2 and the type 3 coppers.

Our spectroscopic studies of the oxidized trinuclear copper site in laccase provide a foundation for a detailed understanding the electronic and geometric structure of this novel active site and the mechanism of the irreversible multielectron reduction of dioxygen to water catalyzed by the multicopper oxidases. The site comprises three tetragonal coppers in which the two type 3 coppers are spectroscopically inequivalent. The antiferromagnetic coupling between the type 3 centers is the dominant magnetic interaction among the coppers, resulting in an $S = {}^1/_2$ ground state in which the paramagnetism is localized on the type 2 site. However, a spin-coupling model indicates that moderate exchange couplings between the type 2 site and the type 3 coppers may exist. A key

(49) (a) Morpurgo, L.; Calabrese, L.; Desideri, A.; Rotilio, G. *Biochem. J.* **1981**, *193*, 639–642. (b) Morpurgo, L.; Agostinelli, E.; Senepa, M.; Desideri, A. *J. Inorg. Biochem.* **1985**, *24*, 1–8.

(50) The wave function for the excited doublet state for positive M is

$$\left|\frac{1}{2}, b\right\rangle = \left(-\frac{1}{\sqrt{2}}\sin\omega + \frac{1}{\sqrt{6}}\cos\omega\right)\left|++-\right\rangle + \left(\frac{1}{\sqrt{2}}\sin\omega + \frac{1}{\sqrt{6}}\cos\omega\right)\left|+-+\right\rangle + \left(-\frac{2}{\sqrt{6}}\cos\omega\right)\left|-++\right\rangle$$

and the corresponding weighting coefficients are given by

$$c_2 = \sin^2\omega - \frac{1}{3}\cos^2\omega \qquad c_{3\alpha} = \frac{2}{3}\cos^2\omega - \frac{2}{\sqrt{3}}\sin\omega\cos\omega$$

$$c_{3\beta} = \frac{2}{3}\cos^2\omega + \frac{2}{\sqrt{3}}\sin\omega\cos\omega$$

(51) Bkouche-Waksman, I.; Boillet, M. L.; Kahn, O.; Sikorav, S. *Inorg. Chem.* **1984**, *23*, 4454–4459.

(52) Velthuizen, W. C.; Haasnoot, J. G.; Kinneging, A. J.; Rietmeijer, F. J.; Reedijk, J. *J. Chem. Soc., Chem. Commun.* **1983**, 1366–1368.

structural feature of the site is the bridged binding of exogenous ligands between the type 2 and each of the type 3 coppers. It is now important to extend these studies in order to probe the interactions of exogenous ligands with the trinuclear site in partially reduced, catalytically relevant oxidation states and to directly characterize the structures of the bound oxygen intermediates in both native and T1Hg laccase.

Acknowledgment. We are grateful to the National Institutes of Health for support (Grant AM31450) P.A.C. acknowledges the National Institutes of Health for a postdoctoral fellowship (Grant GM13606). We thank Georgia Papaefthymiou for assistance with the SQUID magnetometer at MIT and Professor Christopher Reed and Robert Orosz for assistance with the magnetometer at U.S.C. We thank Dr. Peter Sandusky for assistance with the initial T1Hg experiments, Edward Yang for providing the met-T2D sample, and Professor Dean E. Wilcox for assistance in obtaining the met-T2D susceptibility data.

Registry No. Cu, 7440-50-8; laccase, 80498-15-3; azide, 14343-69-2.

Binuclear Electron Reservoir Complexes. Synthesis, Stabilization, and Electronic Structures of the 36- and 37-Electron Complexes $[\{Fe(C_5R_5)\}_2(\mu_2,\eta^n\text{-}C_{10}H_8)]^{m+}$ (R = H, Me): From Biphenyl (m = 1 and 2, n = 12) to Bicyclohexadienylidene (m = 0, n = 10)

Marc Lacoste,[†] Hassan Rabaâ,[‡] Didier Astruc,*[,†,⊥] Nicole Ardoin,[†] François Varret,[§] Jean-Yves Saillard,*[,‡] and Albert Le Beuze[‡]

Laboratoire de Chimie Organique et Organométallique, URA CNRS No. 35, 351 Cours de la Libération, 33405 Talence Cédex, France, Laboratoire de Chimie du Solide et Inorganique Moléculaire, Université de Rennes I, Campus de Beaulieu, 35042 Rennes Cédex, France, and Département de Recherches Physiques, URA CNRS No. 71, Université de Paris 6, 75252 Paris Cédex 05, France. *Received March 9, 1990*

Abstract: The reduction of $[(FeCp)_2(biphenyl)]^{2+}$ ($\mathbf{2a}^{2+}$) was found to be a chemically and electrochemically reversible two-electron process by cyclic voltammetry in DMF at −38 °C. With $LiAlH_4$ this 2e reduction in THF at −80 °C gives an ESR-silent blue species **2**, unstable above −50 °C, the structure of which was searched by using Cp* (Cp* = C_5Me_5). The 2e reduction of the new complex $[(FeCp^*)_2(biphenyl)]^{2+}(PF_6^-)_2$ ($\mathbf{2b}^{2+}$), using Na/Hg in THF at 20 °C gives the ESR-silent stable blue diamagnetic complex **2b**, analogous to **2a**, whereas the cyclic voltammogram of $\mathbf{2b}^{2+}$ shows close reversible one-electron waves. The complex **2b** was shown by ^1H and ^{13}C NMR and Mössbauer spectroscopy to have a 36e Fe_2^{II}bicyclohexadienylidene structure. Comproportionation (K = 172 at 20 °C) was achieved by mixing $\mathbf{2b}^{2+}(PF_6^-)_2$ and **2b** in THF at 20 °C, which gives an 80% yield of the green mixed-valence complex $\mathbf{2b}^+$. The latter is a 37e complex with a weak distortion of the biphenyl ligand and showed 3g values in ESR characterizing a Fe^IFe^{II} complex. Its Mössbauer spectra at 0 field are essentially temperature independent and only contain one quadrupole doublet between 4 and 293 K with an isomer shift and a quadrupole splitting intermediate between those of Fe^I and Fe^{II} monomeric units. This indicates an average valence structure with delocalization or fast electron hopping. Under a field of 6 T, an isotropic value of −3.3 T is obtained for the saturation hyperfine tensor [A]. For the latter, an expected orbital contribution of −0.4 T, mainly representing the contact term, corresponds to 25% of the total spin density on the biphenyl ligand of $\mathbf{2b}^+$. SCF–MS–Xα calculations on $\mathbf{2a}^{2+}$, $\mathbf{2a}^+$, and **2a** show that, when $\mathbf{2a}^{2+}$ is reduced, the first electron transfer involves a metallic b_u level, which has some π_{CC} antibonding character between the two atoms linking the phenyl rings. The second electron transfer is accompanied by a significant increase of this π_{CC} antibonding character. A decreasing of the π_{CC} bonding character of the highest occupied levels of a_g symmetry is also noted. Additional calculations on $\mathbf{1a}^{2+}$ $[Fe_2(\mu^2,\eta^{12}\text{-fulvalene})(biphenyl)]^{2+}$ ($\mathbf{1a}^{2+}$) (isomer of $\mathbf{2a}^{2+}$) indicate that, in contrast to the unoccupied b_u biphenylic level of $\mathbf{2a}^{2+}$, the corresponding fulvenic b_u level is too high in energy to be accessible. Consistently, the reduction of $\mathbf{1a}^{2+}$ is essentially a metal reduction, whereas the reduction of $\mathbf{2a}^{2+}$ can be considered as only involving the biphenyl ligand. Altogether, an accurate determination of the electronic and structural transformation (including their orbital description and thermodynamic estimation) that occurs upon each ET of a fast, reversible 2e-transfer process is reported for the first time, which allows for understanding and thus designing of fast 2e-transfer reagents.

Introduction

The investigations of the electronic structure of mixed-valence bi-[1] and polynuclear[2] inorganic complexes have provided much insight regarding intramolecular electron and charge transfer or delocalization.[1-3] Organic ligands such as fulvalene in biferrocene[4,5] also bring about analogous problems of localization vs delocalization of the mixed valence.[5] The information gained from these studies is of potential use in applied areas such as solar energy storage,[6] where intramolecular electron transfer is a key step. Hendrickson has shown that the lattice, i.e., the counteranion,

[†] Laboratoire de Chimie Organique et Organométallique.
[‡] Laboratoire de Chimie du Solide et Inorganique Moléculaire.
[§] Département de Recherches Physiques.
[⊥] Present address (until September 30, 1991): Department of Chemistry, University of California, Berkeley, CA 94720.

(1) (a) Holm, R. H. In *Biological Aspects of Inorganic Chemistry*, Addison, A. W.; Cullen, W. R.; Dolphin, D.; James, B. R., Eds.; Wiley: New York, 1977; Chapter 2. Nherland, S.; Gray, H. B. *Ibid.* Chapter 10. (b) Trinh-Toan; Teo, B. K.; Ferguson, J. A.; Meyer, T. J.; Dahl, L. F. *J. Am. Chem. Soc.* **1977**, *99*, 408. (c) Wiegardt, K.; Bossek, U.; Nuber, B.; Wiess, J.; Bonvoisin, J.; Corbella, M.; Vitols, S. E.; Girerd, J.-J. *J. Am. Chem. Soc.* **1988**, *110*, 7398. (d) Connelly, N. G.; Geiger, W. E. *Adv. Organomet. Chem.* **1984**, *23*, 1. (e) Eisenbroich, C.; Heck, J.; Massa, W.; Nun, E.; Schmitt, R. *J. Am. Chem. Soc.* **1983**, *105*, 2905. (f) Sharp, P. R.; Raymond, K. N.; Smart, J. C.; McKinney, R. J. *J. Am. Chem. Soc.* **1981**, *103*, 753.
(2) (a) Geiger, W. E.; Connelly, N. G. *Adv. Organomet. Chem.* **1985**, *24*, 87. (b) Chu, T. T.-H.; Lo, F. Y.-K.; Dahl, L. F. *J. Am. Chem. Soc.* **1982**, *104*, 3409. (c) Ferguson, J. A.; Meyer, T. J. *J. Chem. Soc., Chem. Commun.* **1971**, 623. (d) Kubas, G. J.; Vergamini, P. *Inorg. Chem.* **1981**, *20*, 2667.

0002-7863/90/1512-9548$02.50/0